1-1-1995

Transport of solutes in complex hydrogeological media

Vinod Vallikat
University of Nevada, Las Vegas

Transport of Solutes in Complex Hydrogeological Media

by

Vinod Vallikat

A thesis submitted in partial fulfillment
of the requirements for the degree of

Master of Science

in

Water Resources Management

Department of Geoscience
University of Nevada, Las Vegas
December 1995

The thesis of Vinod Vallikat for the degree of Master of Science in Water Resources Management is approved.

Chairperson, Roko Andricevic, Ph.D

Examining Committee Member, David K. Kreamer, Ph.D

Examining Committee Member, James A. Cardle, Ph.D

Graduate Faculty Representative, Ashok K. Singh, Ph.D

Interim Dean of the Graduate College, Cheryl Bowles, Ed.D

University of Nevada, Las Vegas
December 1995

ABSTRACT

This study presents numerical simulations of conservative solute transport in a complex heterogeneous porous media. A methodology to incorporate all the available information for describing the heterogeneity is developed. A Particle Tracking Random Walk method is used to simulate the solute transport through a heterogeneous hydraulic conductivity field generated based on a bimodal distribution. The effect of bimodal distribution on plume migration is examined and the correlation structures of the concentration field is analyzed.

The numerical results indicate that the plume separates into small blocks and travels at different velocities through the preferential flowpaths. This was also noticed in the breakthrough curves in the form of large tails. The correlation structures displayed a trend, suggesting nonstationarity of the concentration field and the spatial continuity was higher in the transverse directions than the longitudinal direction.

ACKNOWLEDGMENTS

At the outset, I would like to thank Dr. Roko Andricevic, for his constant encouragement, guidance and ideas, which were instrumental to the completion of this study. Special thanks to Mr. Karl Pohlmann, for his ever encouraging enthusiasm, and for the many interesting discussions that helped me in completing this study. Thanks are also due to Dr. James Cardle, Dr. David Kreamer and Dr. Ashok Singh for agreeing to be in my thesis committee. I acknowledge the help of Dr. Anita Singh for the useful discussions about some geostatistical problems and Dr. Robert Mose for promptly answering my questions about the flow model.

Contents

List of Figures

Chapter 1

INTRODUCTION

In the recent years the focus of groundwater studies has changed from estimation of groundwater quantity to groundwater quality, due to an increasing assault by chemicals, radioactive wastes, and pesticides. Groundwater pollution increases the cost of providing clean drinking water. Once a pollutant is discovered it is vitally important to be able to predict its movement. This is a difficult problem because the contaminant migrates through natural geological formations, which are heterogeneous in terms of hydraulic properties, especially hydraulic conductivity. This is also supported by field measurements of hydraulic properties in natural geological formations, which indicate that these properties consistently vary throughout the space in an irregular manner (e.g., Dagan, 1986; Gelhar, 1986). Fluid flow and solute transport through these natural formations display uneven distributions in space and time controlled by the spatial heterogeneity of physical and/or chemical properties. It is thus essential to account for the spatial heterogeneity of these properties in order to predict field-scale flow and solute transport.

The focus in this study is on the heterogeneity of hydraulic parameters, which has

a major influence on the groundwater flow and contaminant migration. Inaccurate description of the subsurface heterogeneity when modeling contaminant transport in ground-water systems can result in inaccurate delineation of the contaminant plume which is required for identifying the areas for remediation. The spatial heterogeneity of hydraulic properties in natural formations is usually complicated, and the available information on this spatial variability is limited. It is therefore impossible to construct a detailed deterministic model that represents the actual heterogeneity of formations. Also, the determination of the continuity of high hydraulic conductivity facies within an area of study is critical in predicting contaminant transport and assessing the potential risk that may result from that migration. A small but continuous geologic feature having only one order of magnitude higher conductivity than the surrounding medium can have a dramatic effect on the behaviour of a contaminant plume. The randomly disconnected small fractures may not generate flow paths, whereas a minute volume proportion of connected high conductivity zones may control the migration and thus may become a major contributor to the potential risk.

In the last decade, a stochastic framework for describing subsurface heterogeneity has emerged (Delhome, 1979; Dagan, 1986; Gelhar, 1986) as a way to account for this inevitable natural geologic heterogeneity. In a stochastic modeling study, the spatially variable hydraulic properties are considered as Space Random Functions (SRF). As a consequence, the dependent variables used in the flow and transport equations (such as ground-water head, velocity, solute concentration etc.) are also SRF's. Using the geostatistical approach, the hydraulic properties at unmeasured locations are simulated by a series of equally likely realizations. These realizations account for the uncertainities at unmeasured locations. By solving the flow and transport equations for the series of equally likely realiza-

tions of the hydraulic properties, the uncertainities in flow and transport due to the limited data can be modeled (Dagan, 1986). This type of subsurface heterogeneity generated is based on the single covariance structure, which means that the subsurface attribute (e.g., hydraulic conductivity, porosity, chemical properties etc.,) is generated based on a single spatial correlation structure inferred from the available data set. However when modeling hydraulic conductivity over a wide range of values from the microdarcies to the darcies in three-dimensional (3D) domains, one expects the interaction of multiple geological and diagenetical processes to produce spatial correlation structures for different range of hydraulic conductivity values. For example, high-conductivity values corresponding to fractures have anisotropy and spatial correlation patterns different from those of median-conductivity values corresponding to sands or low-conductivity values corresponding to impervious shales. The single covariance measure does not distinguish between these different integral scales of hydraulic conductivity values. It is important to account for the correlation of extreme hydraulic conductivity values because it would help in identifying the potential flow paths which is very crucial in accurately delineating the contaminant plume.

In practice, the available field data can be divided into two categories:

1. Hard data: This is the actual measured attribute (eg., hydraulic conductivity, porosity, etc.) at a specific location with a low degree of uncertainity. Unfortunately this type of data are usually sparse.

2. Soft data: This type of data is qualitative or quantitative in nature and has various degrees of uncertainity associated with it. These data include but are not limited to: geophyscial information (e.g., well logging, seismic data), or simply expert judgement. Usually this type of data is available.

It is envisioned that the integration of both the type of data will reduce the uncertainity in the subsurface description which will infact reduce the uncertainity in modeling flow and transport in groundwater systems.

1.1 Literature Review

Several investigators have advocated combining geophysical data with hydrological data to help quantify subsurface heterogeneity. For example, Rubin et al. (1992) and Copty et al (1993) developed a method for using seismic information together with head and hydraulic conductivity measurements at several wells to estimate the hydraulic conductivity field.

The realization that the single convariance structure is inadequate to represent the geological complexities typical of most field sites, has motivated to use other types of geostatistical methods. Desbarats (1987) used indicator geostatistics to generate a random hydraulic conductivity field. He then used Monte Carlo simulations with particle tracking to simulate tracer movement through the simulated media. The contrast in sand to shale conductivity was 10^4. He found that a Fickian model does not adequately describe longitudinal spreading in sand-shale sequences over finite fields owing to channeling of the tracer through high conductivity sands.

Several investigators advocated the use of indicator geostatistics with conditional simulation. In a conditional simulation, the simulation is constrained to maintain field-measured values of the parameter at appropriate points in the field.

Philips and Wilson (1989) have advocated the use of soft geological information in stochastic modeling. They suggest that hydraulic conductivity can be correlated with soft geological information such as grain size or geophysical data. Maps of these kinds of data

can then be used to estimate the statistics of the hydraulic conductivity field.

Rubin et al. (1991) discussed the spatial characterization of subsurface heterogeneity using a multimodal distribution for characterizing the spatial continuity of different geological materials. This is especially needed to deal with cases of multiple facies with widely different porosity/permeability properties such as fractured rock, dolomite aquifers with dissolution channels, or sand formations embedded with clayey lenses. They present the algorithm for implementing this technique, which is a modification of the Sequential Indicator Simulation (SIS) algorithm of Gomez-Hernandez and Srivastava (1990). Their results of a simulation for a case of perfect stratification, suggest that single-covariance based approach fails to distinguish the different populations present and hence substantiates the need for multimodal distributions for describing the spatial heterogeneity present.

Brannan and Haselow (1993) described a method for incorporating soft geologic information into stochastic simulation. They used multiple indicator functions with associated cutoff levels to define hydraulic conductivity of gelogical materials. The distribution of lnK is assumed to be Gaussian within each geological unit defined by an indicator. The indicators can be defined at several scales from the microscale to the scale of facies and facies assemblages up to the regional scale of the hydrostratigraphic unit. The method generates lenses of geological units either randomly or constrained (conditioned) by the use of soft data. The constraints may include information on the geometry and orientation of the lenses for each indicator category.

Ritzi et al. (1994) used conditional indicator simulation to produce realizations of an outwash deposit in a buried-valley system in Ohio, USA. They assumed that the aquifer could be represented by two facies types: a low-permeability facies consisting of till or

lacustrine clay and a high-permeability facies consisting of sand and gravel outwash deposits. They used the computer code ISIM3D devloped by Gomez-Hernandez and Srivastava (1990) to generate multiple realizations of the aquifer.

Wingle et al. (1994) developed a computer code (UNCERT) that is a geostatistical uncertainity analysis package for groundwater flow and contaminant transport modeling. The philosophy used to build UNCERT stresses the importance of integrating all available data, including hard, soft and fuzzy data, in order to constrain the results as much as possible.

1.2 Thesis Outline and Objectives

In this thesis, numerical simulations are performed in order to address the following issues:

1. Develop a procedure to incorporate both hard and soft data for description of subsurface heterogeneity.

2. Examine the effect of bimodal distribution of spatial characterization on plume migration.

3. Examine the correlation structures of hydraulic conductivity field, velocity field, and concentration field.

In chapter 2, the general setting of the area under study, the geographic and geologic description, and the data availability are discussed. The details of the methods used in this study are presented in Chapter 3, which includes the theory of Indicator Statistics and Sequential Indicator Simulation technique, the generation of hydraulic conductivity field using both hard and soft information, a short review of the theory of flow modeling and the

details of the Particle Tracking Random Walk method used for transport simulations. In chapter 4, the problem formulation for numerical simulations is defined, method of analysis is discussed and the results are presented.

Chapter 2

SITE DESCRIPTION

In this chapter, the general setting of the area under study, the geographic and geologic description and also the data availability will be discussed.

2.1 Geographic and Geologic Description

The Nevada Test Site (NTS), Figure 2.1, is located about 105 kilometers (65 miles) northwest of Las Vegas, Nevada and has an area of about 349650 hectares (1350 sq. miles) in Nye county. Yucca Flat (Figure 2.2) is an alluvium filled valley in the east central portion of the NTS, was the site of five hundred and forty-eight underground nuclear tests (U.S. Department of Energy, 1991, pg. v).

The hydrogeologic conditions and data availability were used to define the problem domain and its orientation in space. An area covering parts of the Nevada Test Site (NTS) Areas 1, 3, 4 and 7 in Yucca Flat shown in Figure 2.3 is chosen for this purpose. The area contains 24 wells that all had lithologic and extensive geophysical logs (Table 2.1).

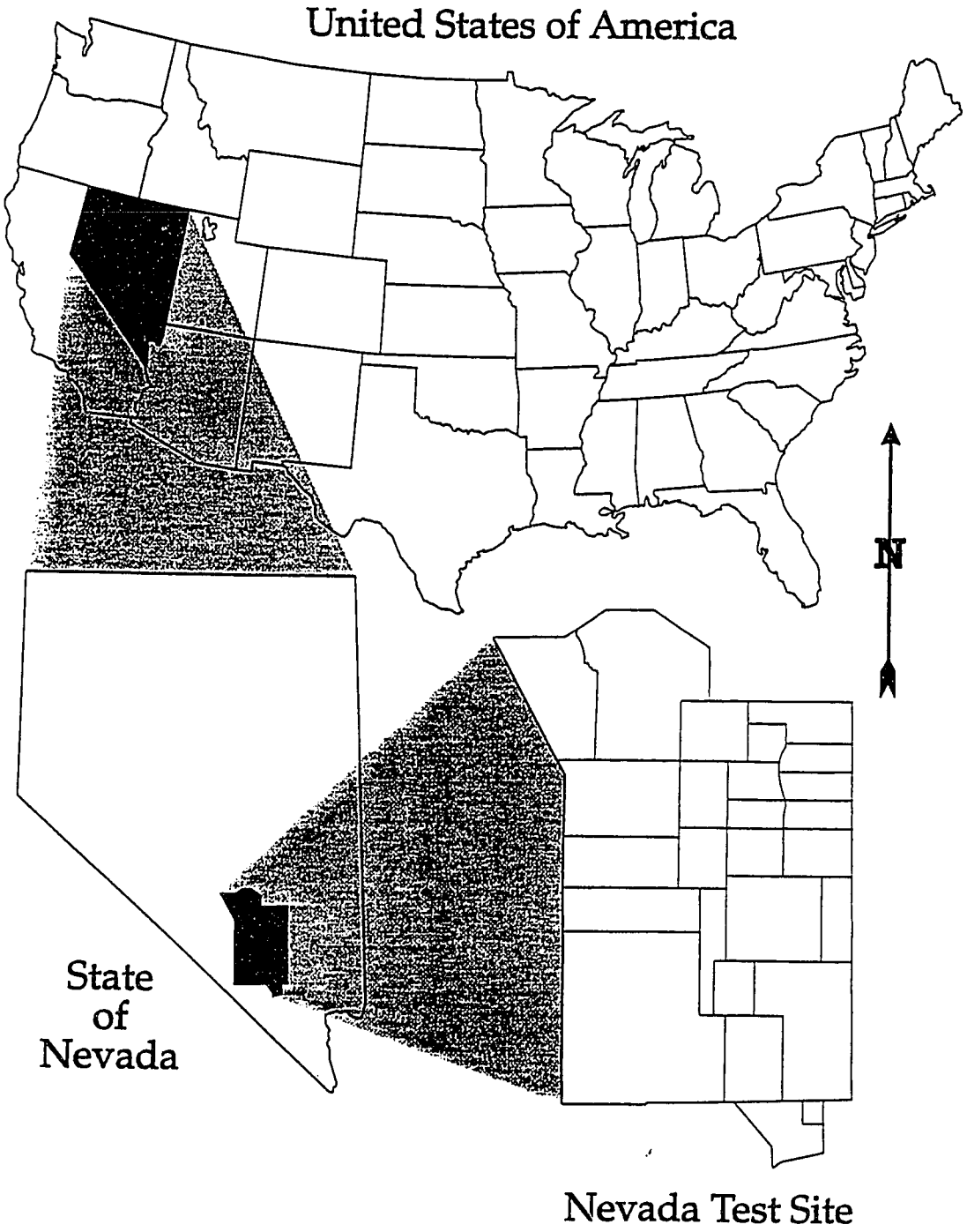

Figure 2.1: Location map of Nevada Test Site (NTS)

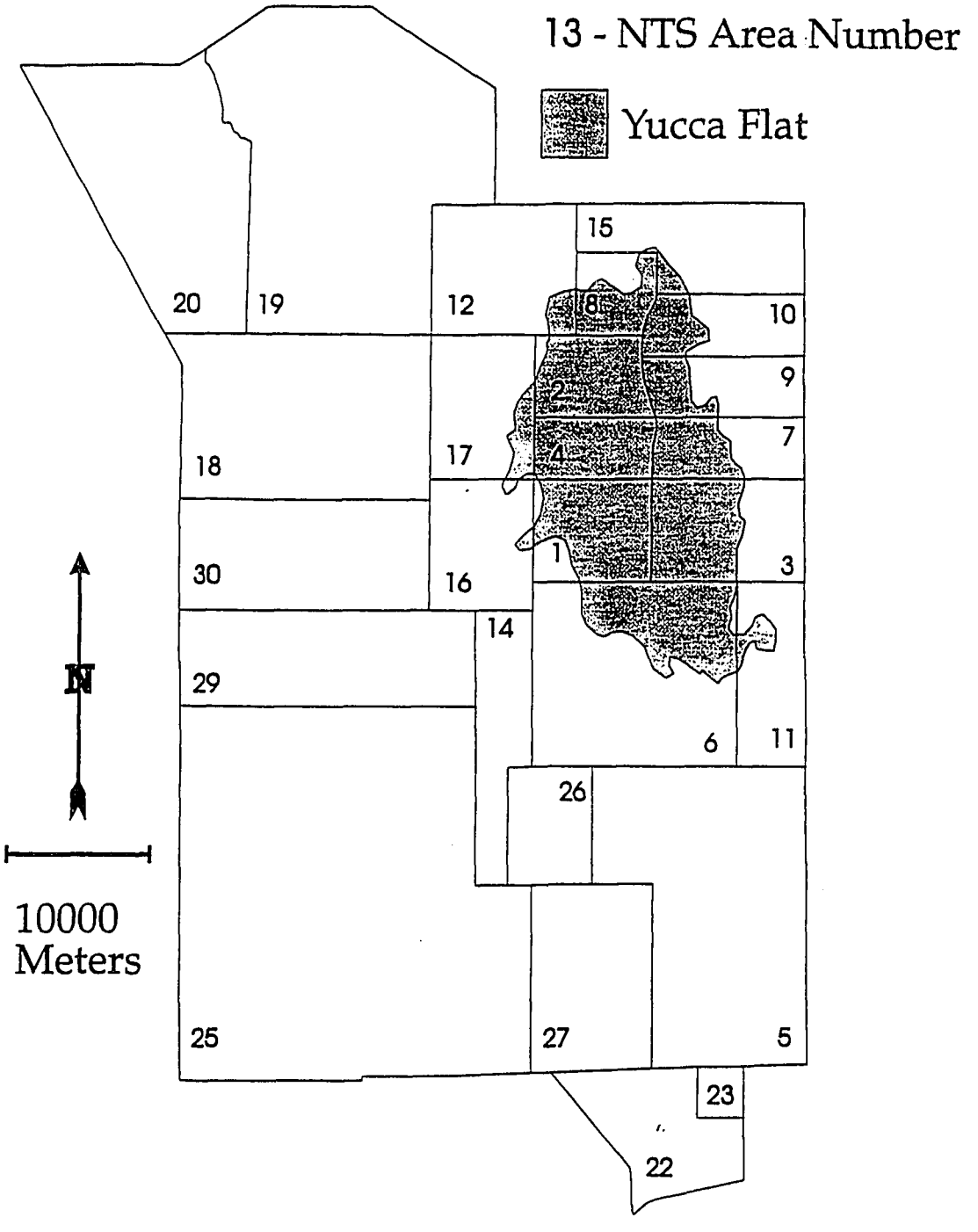

Figure 2.2: Location map of Yucca Flat, NTS showing numbered test areas

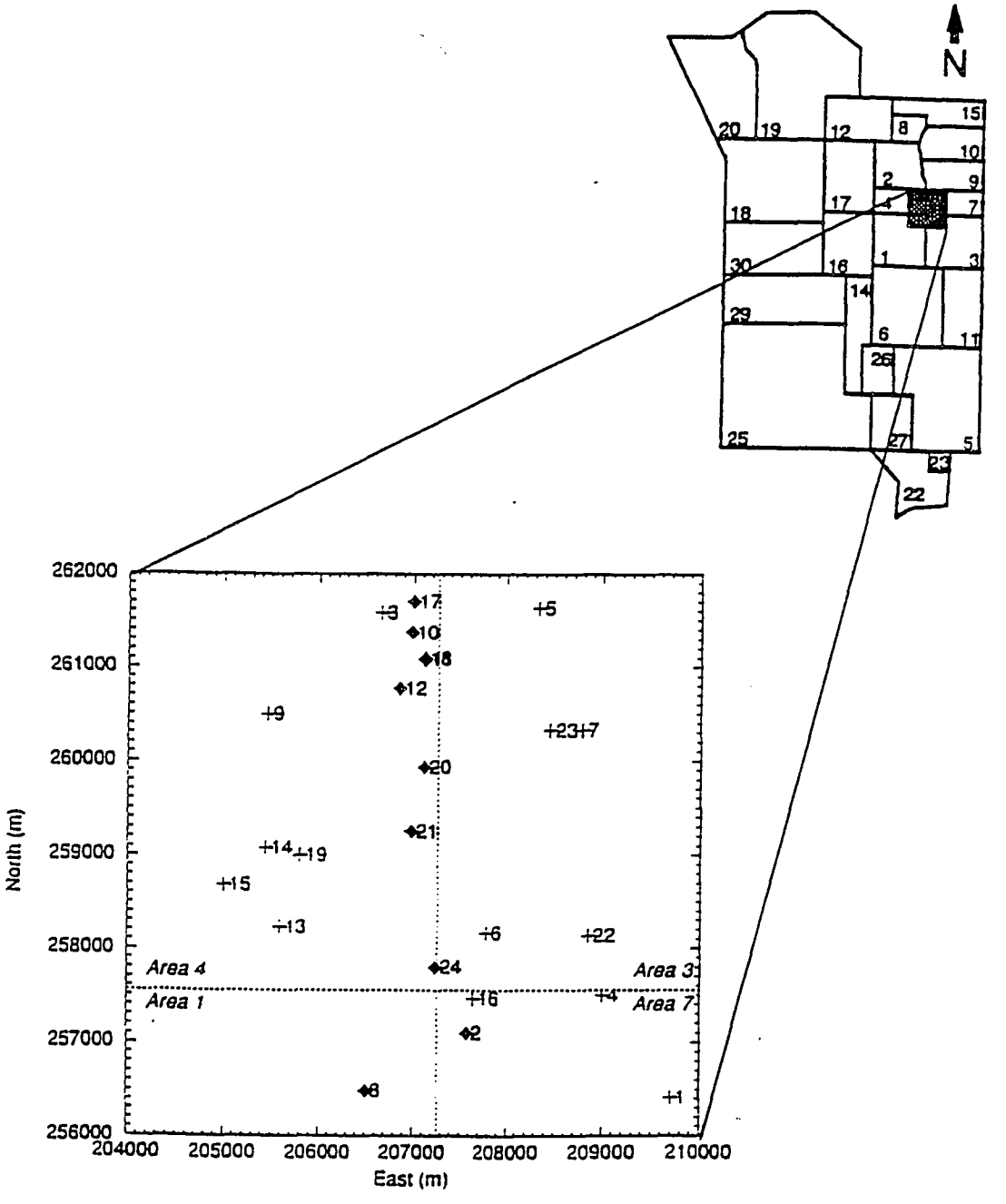

Figure 2.3: Location of study area and plan view of well locations. Wells indicated by diamonds have been projected on a cross section at x=207,000 m.

Table 2.1: Wells Used in this Study

Well ID	NTS Well Name	Easting (m)	Northing (m)
1	U 3cn	209702.2	256415.0
2	U 3gg	207569.2	257099.0
3	U 4e	206654.8	261580.2
4	U 7ai	209001.5	257495.9
5	U 7ak	208327.9	261634.7
6	U 7an	207782.6	258166.1
7	U 7bs	208788.84	260330.2
8	UE 1q	206502.4	256489.7
9	UE 4av	205459.1	260494.8
10	UE 4d1	206971.2	261376.0
11	UE 4g2	207126.9	261092.2
12	UE 4t	206847.7	260776.7
13	UE 4ae	205588.0	258227.1
14	UE 4ah	205435.6	259080.5
15	UE 4al	204999.7	258684.3
16	U 31a	207640.8	257465.1
17	U 4a	206989.8	261702.7
18	U 4g	207111.7	261092.7
19	U 4i	205801.4	259000.7
20	U 4j	207111.7	259934.3
21	U 4r	206976.4	259254.9
22	U 7ac	208849.4	258135.6
23	U 7ah	208453.7	260330.2
24	U 7aq	207234.2	257800.3

Yucca Flat is a typical Basin and Range graben containing up to 600 m of Quaternary alluvial valley fill derived from the surrounding mountain blocks. The alluvium is generally unsaturated in Yucca Flat. Underlying the alluvium is a thick sequence of Tertiary volcanic rocks consisting of air-fall, ash-flow, and reworked tuffs. Densely-welded ash-flow tuffs and vitrophyres within the upper portion of this section tend to be fractured, and when deep enough to be saturated, are considered aquifer (the "welded-tuff" aquifer of Winograd and Thordarson, 1975). Although the welding of these units reduces matrix porosity to very low values, it also causes them to be subject to fracturing. Connected fracture zones

within densely-welded tuffs and/or vitrophyres may create pathways for groundwater flow.

Air-fall and ash-flow tuffs below the densely-welded ash-flow tuffs tend to be non-welded or partially welded and are generally zeolitized. Although matrix porosity of these units may be high, most pores are unconnected, so the effective porosity is low. In addition, the clay and zeolite matrices of these rocks tend to reduce the interstitial hydraulic conductivity to very low values. Finally, nonwelded tuffs contain few fractures so they are unlikely to act as important flow paths. Taken as a whole, these tuffs comprise the "tuff aquitard" that restricts movement of groundwater below Yucca Flat (Winograd and Thordarson, 1975). The tuff aquitard is bounded below by Paleozoic rocks that form an important aquifer/aquitard system that defines the regional flow of groundwater (Winograd and Thordarson, 1975). A simplified north-south hydrogeological cross section at x =207,000 m is presented in Figure 2.4, (data from Drellack and Thompson, 1990). Data from the wells shown are projected on the section, while the upper surface of the carbonates is derived from a contour map of the area. CWL is the composite water level measured in the boreholes.

2.2 Data Availability and Problem Formulation

At the Nevada Test Site, there is an important need to identify potential flowpaths for groundwater movement. For any site, it would be ideal to have large amount of direct measurements of hydraulic conductivity values (hard data) in order to realistically characterize the domain. However, the availability of hard K data at most sites is very limited. As an alternative, some of these sites may have a great deal of soft data available. The choice of the type of soft data to be used as the subsurface attribute depends on the data availability

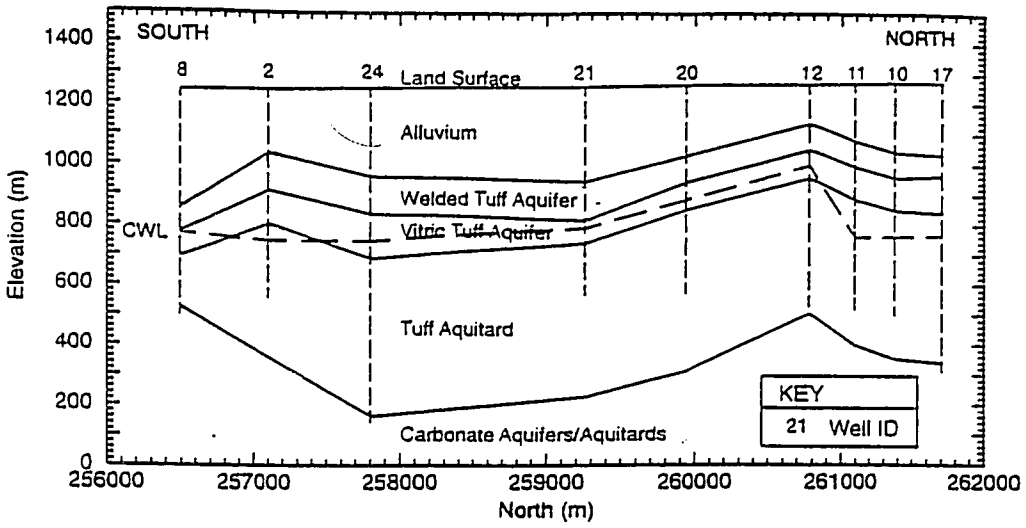

Figure 2.4: North-south hydrogeologic cross section at x = 207,000 m

and the relationship between the soft data "signal" and the hydrogeologic variable of interest. For example, some types of soft data, such as lithologic logs and geologic maps, may have low spatial resolution and little direct relation to hydraulic conductivity. On the other hand, certain geophysical logs may provide information on the nature of the hydrogeologic units and therefore may provide relatively direct information on hydrogeologic variables. In the case of Yucca Flat, very little hard K data are available, but there is a very large amount of geophysical log data available.

Three geophysical logs that may be useful to the description of hydrogeologc variables in the volcanic units at Yucca Flat are the gamma-gamma ("density") log, neutron ("porosity") log, and the resistivity ("electric") log. The brief description of these logging methods presented here is based on Keys (1990) and Drellack(1994). The relation of the logs to NTS geology is based on the work of Drellack (1994). The gamma-gamma log uses a gamma radiation source to measure electorn density in the formation. Electron density is

approximately proportional to bulk density for most rocks and the higher the bulk density, the more the gamma signal is attenuated. The bulk density can be converted to an estimate of porosity if fluid and grain density are known, although effective porosity is difficult to distinguish from total porosity. The gamma-gamma signal in volcanic rocks on the NTS is primarily a function of porosity and welding, and to a lesser extent, mineral alteration. Porosities of ash-flow tuffs range up to fifty (50) percent while porosities in a densely-welded vitrophyre may be as low as three percent. While porosity decreases as degree of welding increases, grain density increases with increasing degree of welding. Therefore, densely-welded ash-flow tuffs generally can be distinguished from non-welded tuffs by their higher gamma-gamma (density) signal. If densely-welded tuffs are significantly fractured, they may represent zones of high relative K, and therefore may be potential pathways of groundwater flow.

The neutron logging tool emits neutrons and records their interactions with adjacent rocks. The number of these interactions is controlled by the quantity of hydrogen present, which is a function of the water content. In a fully saturated rock a low neutron count generally indicates high porosity, as a result of the high proportion of the rock volume occupied by water molecules. As with the gamma-gamma log, the neutron log cannot distinguish between total and effective porosity. At the NTS, volcanic rocks with higher density or lower porosity generally have lower water content and therefore usually exhibit high neutron signals. These conditions may indicate a fractured, densely-welded tuff that may be a potential pathway for groundwater flow. In contrast, volcanic rocks that have high porosity (air-fall and nonwelded ash-flow tuffs) and/or are altered by zeolitization usually exhibit low neutron signals (high apparent water content). These rocks generally

are considered to have very low hydraulic conductivity.

The resistivity tool measures the resistance of a volume of rock to the flow of an electrical current. Most rocks are not good conductors of electricity so resistivity is a function of the resistance and volume of pore water. The resistivity log is a measure of effective porosity because the electric current can flow only through connected pores. The resistance of pore water in the tuffs at Yucca Flat is fairly uniform and is relatively high due to its low dissolved solids content. Therefore, the resistivity of tuffs at Yucca Flat is primarily a function of porosity. Air-fall and nonwelded ash-flow tuffs have high porosity and exhibit low resistivity. As the degree of welding increases, the porosity is reduced and the resistivity increases. Densely-welded tuffs and rhyolite lava flows have the highest resistivities. Zeolitization has the effect of lowering apparent resistivity in all tuffs because the pore water has lower resistance. As a result of these relationships, a high resistivity response is likely to indicate a potential pathway of groundwater flow, while a low response is likely to indicate a potential barrier to groundwater flow.

All three of the geophysical logs described above may be suitable for soft data simulation because they all can be used to differentiate between densely-welded tuffs and nonwelded tuffs. However, interpretation of the gamma-gamma and resistivity logs appears to be most straightforward. Numerical ranges for values of bulk density (derived from the gamma-gamma log) and resistivity typical of selected rock types on the NTS are shown in Table 2.2 (Drellack, 1994). Potential flow paths, if assumed to be represented by densely-welded tuffs and vitrophyres, exhibit an easily identifiable and distinct response on these logs. Air-flow tuffs, nonwelded ash-flow tuffs, and zeolitized tuffs, which are assumed to represent potential barriers, exhibit a distinctly different response in each log.

Resistivity logs were chosen for this study because of their availability and relative ease of interpretation. Blankennagel and Weir (1973) also used resistivity logs to differentiate permeable densely-welded tuffs and vitrophyres from relatively impermeable zeolitized tuffs. They used a threshold resistivity value of 225 ohms-m^2/m.

Table 2.2: Values of Bulk Density and Resistivity at Yucca Flat

Rock type	Bulkdensity (g/cc)	Apparent Resistivity (ohm-m^2/m)
Alluvium	1.60 - 1.80	20 - 300
Ash-Flow Tuffs		
Nonwelded	1.40 - 1.75	110 - 750
Partially to Moderately Welded	1.75 - 2.20	145 - 650
Densely Welded	2.20 - 2.40	700 - 1000
Air Fall Tuffs	1.60 - 2.20	20 - 100
Paleozoic Rocks	2.20 - 2.85	40 - 200

For this work 300 ohm m^2/m was chosen as threshold value in order to represent only the more densely-welded tuffs. Based on the relationships presented in Table 2.2, resistivity values above this threshold represent moderate-to densely-welded tuffs and values below this threshold represent non-welded tuff units. Welded tuff units tend to be fractured. Although the matrix porosity is very low due to welding, when these fractured units are connected, they may act as potential flowpaths for groundwater flow.

Chapter 3

Methodology

In this chapter the methodology adopted in this study is discussed in detail. The flow chart given in Figure 3.1 shows the various tasks involved and the order of implementation.

Section 3.1, includes a short review of the Indicator geostatistics, the theory of Sequential Indicator Simulation (SIS), and the implementation of this technique. Also included are the details of inclusion of soft data, using the indicator approach. In Section 3.2, the details of Hydraulic conductivity field generation using both soft and hard information is presented. A short review of the statistical representation of hydraulic conductivity and correlation structure is also included for completeness. Section 3.3 provides in brief, the theory of flow modeling and the program used to obtain the velocity field. Finally, in Section 3.4, the Particle Tracking Random Walk method used to simulate contaminant transport is discussed.

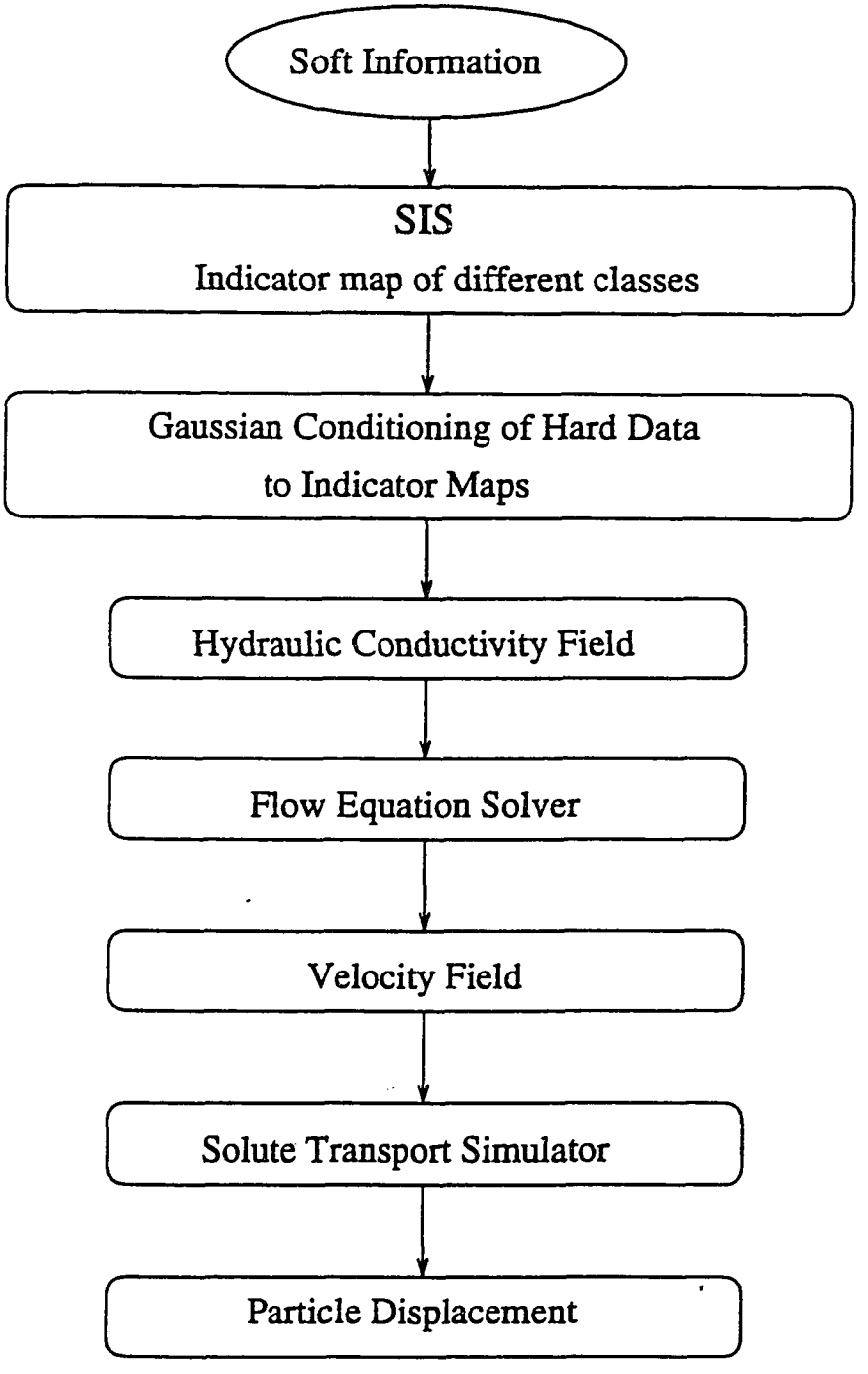

Figure 3.1: Steps involved in numerical simulation of solute transport

3.1 Indicator Geostatistics

The indicator formalism has been introduced in the field of spatial statistics by Switzer (1977). Most of the recent extension and developments are due to Journel (1989) and Journel and Alabert (1988). Indicator geostatistics involves the discretization of data into classes. Thus instead of working with actual values of the attribute $Z(x)$, as in parametric geostatistics, a nonparametric approach considers the indicator values, $I(x; z_c)$ defined as

$$I(x; z_c) = \begin{cases} 1 & \text{if } Z(x) \leq z_c \\ 0 & \text{if } Z(x) > z_c \end{cases} \tag{3.1}$$

where $I(x, z_c)$ is the indicator values, with possible outcomes of 0 or 1, and z_c is the threshold value. The indicator has a value of one if the value of the variable is less than or equal to the threshold, and a value of zero if the value of the variable is greater than the threshold. By using L threshold values, z_{ck}, $(k =, 1, ..., L)$, the range of $Z(x)$ is subdivided into $L + 1$ classes. The threshold values may be dictated by a regulatory body (as in the case of contaminant levels), may be determined from the field data, or may rather arbitrarily be set to the quartiles or deciles of a continuous distribution.

The indicator formalism offers several advantages. First of all, the transformation to indicator classes can be done on any shape of data distribution. Secondly, non-numeric data can be analyzed and modeled through indicator geostatistics. For example, hydrofacies or "non-detect" data in a geochemical sampling survey. Thirdly, the indicator treatment does a better job of retaining extreme values present in a data set relative to other estimation procedures. For example, several extreme data values in a log-normally distributed gold assay data distribution can be modeled as a separate indicator class. This class would

be retained in simulations and not smoothed away as is done in estimation through a standard kriging procedure or some other smoothing technique (Figure 3.2), which shows the comparison of estimation and simulation results in one-dimension. The eight circles denote sample locaitons. Estimation produces a curve which is, on average, closer to reality but is overly smoothed relative to reality. Simulation produces a curve which better captures the variability of reality (Journel and Huijbregts, 1978). Lastly, and very important for the current study, the transformation of data into indicators is currently the only means by which the use of subjective or "soft" information can be incorporated into geostatistical calculations.

The main properties of Indicator Random Functions are briefly recalled in this section. The expected value of $I(x; z_c)$ is equal to the value of the cumulative probability distribution of $Z(x)$ at z_c; that is the proportion of $Z(x)$ which is below z_c, i.e.,:

$$E\{I(x; z_c)\} = 1 \times P\{Z(x) \leq z_c\} + 0 \times P\{Z(x) > z_c\} = P\{Z(x) \leq z_c\} = F(z_c) \qquad (3.2)$$

The expected value of the product $I(x_1; z_c)$ and $I(x_2; z_c)$, gives the noncentered covariance, which is the value of the bivariate distribution of $Z(x)$ for locations x_1 and x_2 and the threshold z_c:

$$E\{I(x_1; z_c)I(x_2; z_c)\} = P\{Z(x_1) \leq z_c; Z(x_2) \leq z_c\} = F(h; z_c) \qquad (3.3)$$

where $h = |(x_1 - x_2)|$ is the separation vector of $I(x_1; z_c)$ and $I(x_2; z_c)$.

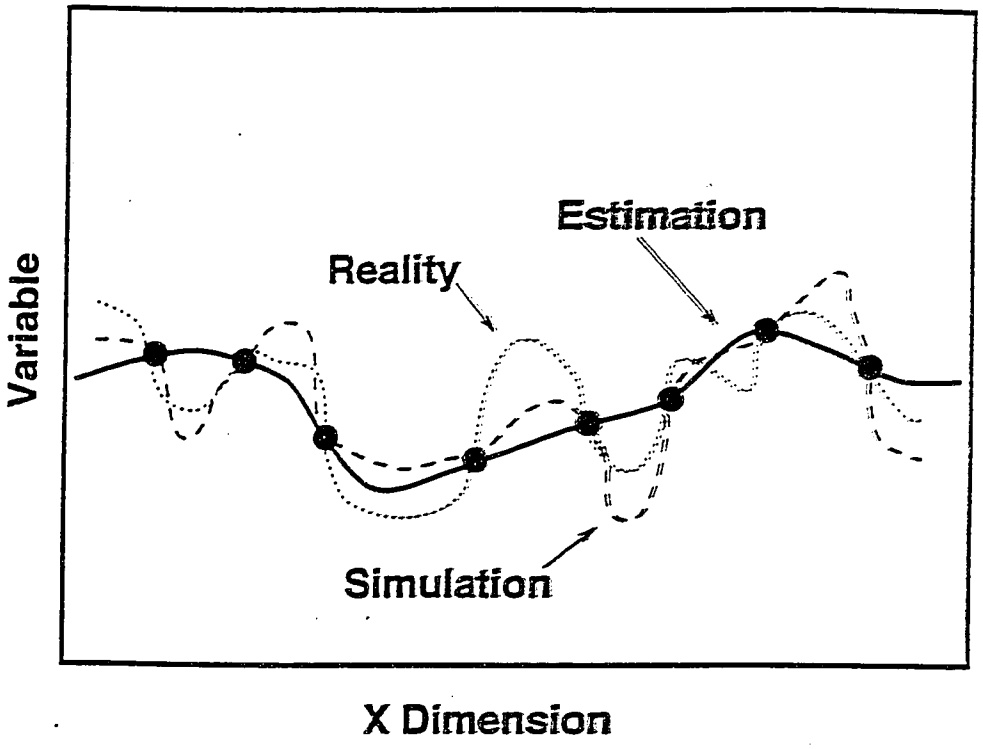

Figure 3.2: A comparison of estimation and simulation results in one-dimension (after Journel and Huijbregts, 1978)

Thus the indicator covariance is:

$$C_I(h; z_c) = E\{[I(x_1; z_c) - F(z_c)][I(x_2; z_c) - F(z_c)]\} = F(h; z_c) - F^2(z_c) \qquad (3.4)$$

with indicator variance

$$Var\{I(x; z_c)\} = C_I(0, z_c) = F(z_c) - F^2(z_c). \qquad (3.5)$$

The indicator semivariogram is:

$$\gamma_I(h; z_c) = 0.5 \times E\{[I(x_1; z_c) - I(x_2; z_c)]^2\} = F(z_c - F(h; z_c). \qquad (3.6)$$

Equation 3.3 is a measure of two-point spatial continuity. The higher this value, the greater the probability of having two values $Z(x_1)$ and $Z(x_2)$ which jointly do not exceed the same threshold value z_c (Journel and Alabert, 1990). Thus, for different thresholds, the indicator covariance (3.4) or indicator variogram function (3.6) account for the structures of spatial continuity at different thresholds. The larger the correlation scale in the indicator variogram, the better the spatial continuity of the threshold value.

Based on the indicator data and indicator statistics (moments, variogram) at each threshold, the realizations of $Z(x)$ can be generated using the Sequential Indicator Simulation (SIS) algorithm (Gomez-Hernandez and Srivastava, 1990).

The basic ideas of SIS are given by Alabert (1987) and Journel (1989). It is an application of Bayes's theorem. In SIS, the nodes in the modeling domain A are informed sequentially; the posterior cumulative distribution at the informed point x, conditioned

to the prior indicator data at each threshold is calculated by using the indicator kriging (Journel, 1983, 1989), ie.,:

$$P\{Z(x) \leq z_{ck}|(N)\} = E\{I(x; z_{ck})|(n)\}, k = 1, ..., L \tag{3.7}$$

and

$$E\{I(x; z_{ck})|(N)\} = \sum_{i=1}^{N} \lambda_i(x; z_{ck}) I(x_i; z_{ck}) \tag{3.8}$$

where N is the conditional indicator data number at threshold z_{ck}, x is the coordinate of the informed node. $\lambda_i(x; z_{ck})$, is the indicator kriging weights which are functions of both the threshold values z_{ck} and the location x.

A value of $Z(x)$ at the informed point x is drawn randomly from this estimated posterior distribution and is then added to the set of simulated values. The original data is honored and the indicator variogram at each threshold value is accounted for by the kriging system in 3.8.

Journel and Alabert (1988) published the original description of the Sequential Indicator Simulation (SIS) algorithm. The implementation of the algorithm is given by Gomez-Hernandez and Srivastava (1990). The following description of the algorithm is based on these two publications.

3.1.1 Mechanics of Simulation

Figure 3.3 is a flow chart of the original SIS algorithm and its implementation in the computer program ISIM3D, a three-dimensional, multiple indicator, conditional simulation program developed by Gomez-Hernandez and Srivastava (1990).

The conditioning data are read and transformed into the corresponding indicator values based on thresholds determined by the user. Variogram parameters are read in for each indicator. Then all possible indicator covariance values are calculated and stored.

The simulation consists of the following steps:

1. A random path is defined through all the nodes to be simulated. The simulations proceeds sequentially along this path with the operations described below implemented at each node to be simulated.

2. The conditioning data present within a given search neighborhood are identified and the closest data points are retained for kriging.

3. For each indicator threshold, a kriging system using the indicator semivariogram model is set up and solved.

4. The kriging weights are used to compute the conditional probability distribution function (cpdf) using the indicator conditioning data for the current threshold. The cpdf provides the probability that the value of the attribute at the present node does not exceed the threshold value, in other words, the probability that the attribute is in the lower class.

5. A uniform random number between zero and one is drawn. If the number is less than or equal to the cpdf at the current node, the node is assigned to the lower class with an indicator of one. Otherwise, the node is assigned to the higher class with an indicator of zero.

6. The node just simulated is then included in the conditioning data set and the simulation proceeds.

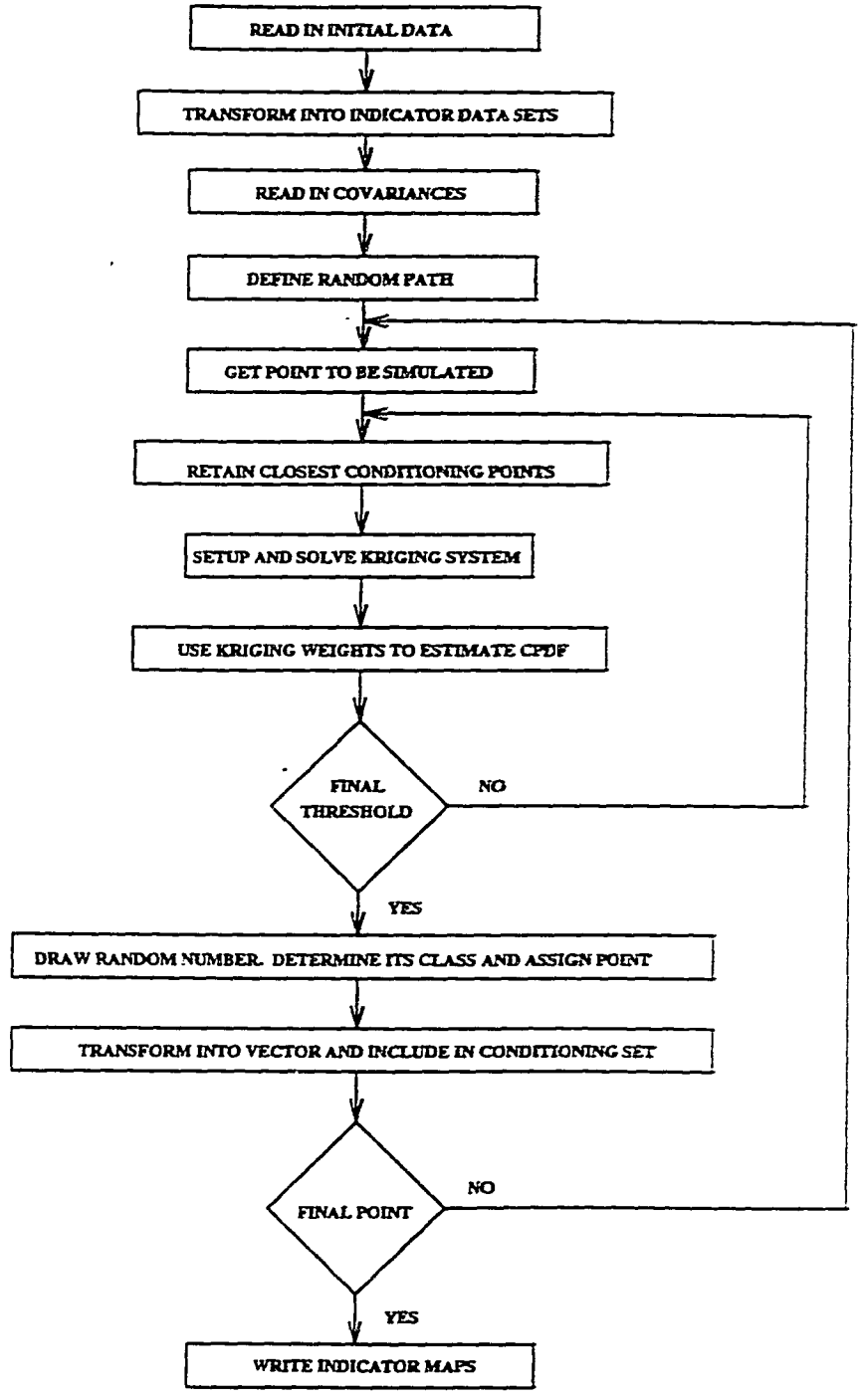

Figure 3.3: Flow chart of the implementation of the SIS algorithm in the program ISIM3D (After Gomez-Hernandez and Srivastava, 1990)

7. When all the points have been simulated, the resulting indicator map is written.

This technique of Sequential Indicator Simulation will be used to generate equiprobable maps of the subsurface using the soft information available, which otherwise cannot be incorporated in the description of the subsurface. The output from this program will be an indicator map of the subsurface defining each node to a particular class.

3.2 Hydraulic Conductivity field

The hydraulic conductivity may be defined as a "combined property of the porous medium and the fluid flowing through it" and gives an indication of the "ability of aquifer material to conduct water through it under hydraulic gradients" [Bear, 1972]. The hydraulic conductivity, K, is dependent on the geometry of the porous medium through the permeability, κ, and dependent on the fluid through the kinematic viscosity, ν, following

$$K = \frac{\kappa \cdot g}{\nu} \tag{3.9}$$

where g is the acceleration of gravity. The dimension of K is length $\cdot$ time^{-1}. In natural formations the hydraulic conductivity is anisotropic and therefore exhibits a tensorial property

$$K = \begin{vmatrix} K_{11} & K_{12} & K_{13} \\ K_{21} & K_{22} & K_{23} \\ K_{31} & K_{32} & K_{33} \end{vmatrix} \tag{3.10}$$

If the Cartesian coordinate axes are aligned with the principal axes of hydraulic conductivity, K is reduced to three diagonal components, K_1, K_2, and K_3. For the sake of simplicity,

and without loss of generality, this alignment is assumed for the remainder of this work.

3.2.1 Statistical Representation

Since natural formations do not possess uniform properties over large areas and sufficient data are usually not available to completely describe the small-scale variability, many researchers represent the hydraulic conductivity as a stochastic random field.

Many investigators have concentrated on finding the pdf which best describes the spatial distribution of the hydraulic conductivity field, $K(x)$. Freeze (1975), summarized many years worth of field measurements and a large body of laboratory work and concluded that the log-normal distribution seems to fit hydraulic conductivity field data. Since then, numerous other investigators have supported this conclusion. Hoeksema and Kitanidis (1985) analyzed hydrogeological properties from 31 regional aquifers and found the natural logarithm of the hydraulic conductivity measurements generally passed normality tests. At present the assumption of log-normally distributed hydraulic conductivity is accepted as a general tenet in natural hydrogeological formations (Dagan, 1989).

If the distribution of $K(x)$ is assumed to be log-normal, then the variable

$$Y(x) = lnK(x) \tag{3.11}$$

is distributed normally, with mean μ_Y and variance σ_Y^2

$$Y(x) : N(\mu_Y, \sigma_Y^2) \tag{3.12}$$

The parameters μ_Y and σ_Y^2 are defined as

$$\mu_Y = E(Y(x)) = E(lnK(x)) \tag{3.13}$$

$$\sigma_Y^2 = E(Y(x) - \mu_Y)^2 = E[lnK(x) - E(lnK(x))]^2 \tag{3.14}$$

where $E()$ denotes expectation. The variance of $lnK(x)$ represents the degree of variability of $K(x)$.

3.2.2 Correlation Structure

Besides using field measurements to describe the randomness of the hydraulic conductivity field, many studies has been conducted, using these measurements to find a correlation structure for $K(x)$. However, this is a difficult task, as large number of measurements is needed, particularly at small distances. Hoeksema and Kitanidis (1985) assumed an exponential correlation function and found that there was good correspondence between it and the measurements of $lnK(x)$. At Borden site, an analysis of the spatial correlation structure of $lnK(x)$ revealed that the correlation function could be approximated as exponential (Sudicky, 1986). Because no conclusive agreement exists, on the most appropriate correlation structure of the hydraulic conductivity, and because it is easy to use, the exponential function is often employed in subsurface flow and transport modeling.

If weak stationarity is assumed for the hydraulic conductivity field then the exponential correlation structure for $lnK(x)$ is a function of the separation distance between two points, x_1 and x_2, not their positions. Let r be the separation distance between x_1 and

x_2

$$r = |x_2 - x_1| = [(r_1)^2 + (r_2)^2 + (r_3)^2]^{1/2} \tag{3.15}$$

where r_i is the separation distance in the i-th principal directions. The spatial correlation of the hydraulic conductivity field is then described by

$$\rho_Y(r) = exp(-[(r_1/\lambda_{Y1})^2 + (r_2/\lambda_{Y2})^2 + (r_3/\lambda_{Y3})^2]^{1/2}) \tag{3.16}$$

where $\lambda_Y(r)$ is the correlation between two points separated by a distance of r and λ_{Yi} is the correlation length of $Y(x)$ in the i-th principal direction. The correlation length is used to parameterize the spatial correlation and is an approximate measure of the distance at which correlation ceases (the correlation becomes zero as the distance between two points approaches infinity). The larger correlation length implies greater spatial continuity in hydraulic conductivity. In this study, correlation length is defined to be equal to the separation distance between two points at which the correlation becomes equal to e^{-1}.

The Sequential Gaussian Simulation (SGS) method is used to combine both the soft information and hard information available to generate the hydraulic conductivity field. Similar to SIS methodology, in the Sequential Gaussian Simulation method also, the nodes in the modeling domain A are informed sequentially. Once a node x_k, has been classified to be in a particular class (from SIS), then the first two moments (μ and σ^2) are obtained by gaussian conditioning (simple kriging) of the hard data available. The data used will be obtained by screening the predefined search neighborhood surrounding the x_k, for nodes which belong to the same population (class) as x_k. The simple kriging estimate and variance then define a normal distribution from which the simulated value $Z(x_k)$ (hydraulic

conductivity) is drawn. This simulated value is included in the conditioning data set and the simulation proceeds. In case there is no hard data available in the search neighborhood, then the global estimates of the first two moments for the particular class at x_k will be used. Finally, this gives the hydraulic conductivity field, conditioned to both the hard and soft information, which will reduce to a very large extent the uncertainity present in the description of the subsurface heterogeneity.

3.3 Velocity Field Calculation

Steady-state flow in saturated porous media is described by Darcy's law:

$$v(x) = -\frac{1}{n}[K(x)\nabla\phi(x)] \tag{3.17}$$

where $v(x)$ is the velocity field, n is the constant porosity, and $\phi(x)$ is the hydraulic head field obtained by solving

$$\nabla \cdot [K(x)\nabla\phi(x)] = 0 \tag{3.18}$$

(in this case fluid density, viscosity, and temperature are considered constant). Once the distribution of the hydraulic conductivity field is obtained, various numerical methods can be used to solve the general flow equation for the hydraulic head, $\phi(x)$. Some of the methods include finite difference, finite element, boundary element, and analytical method. In this study, the Mixed hybrid finite element is employed using the MARFLOW program(Mose et al, 1994; personal communication with R. Mose).

The basic idea in this method is to approximate simulataneously the pressure P and its gradient related velocity field $\vec{q}$. Besides determining the cell pressures P_i it also

calculates the flux Q through the edges, which defines the velocity field at every point. Also the obtained velocity field has a continuous normal component at the interface between two elements.

Once the domain of simulation is defined, the hydraulic conductivity values obtained from the above step is assigned at the center of each cell. The velocities at all the faces of the element are then calculated by the mixed hybrid finite element method.

3.4 Concentration Field

The general equation describing transport of a nonreactive, conservative solute in a three-dimensional saturated porous medium, with constant porosity is

$$\frac{\partial c(x,t)}{\partial t} + \nabla \cdot [c(x,t)v(x)] - \nabla \cdot [D(x)\nabla c(x,t)] = 0 \tag{3.19}$$

where $c(x,t)$ is the concentration (dimension of mass $\cdot$ length^{-3}) and $D(x)$ is dispersion coefficient tensor (dimension of length$^2\cdot$ time^{-1}). The components of $D(x)$ are

$$D(x) = \alpha_T |v(x)| I + (\alpha_L - \alpha_T)\frac{v(x) \cdot v(x)}{|v(x)|} + D_m \tag{3.20}$$

where α_L and α_T are the longitudinal and transverse local dispersitivies (dimension of length), $|v(x)|$ is the magnitude of the velocity, I is the identity matrix, and D_m is the coefficient of molecular diffusion (dimension of length$^2\cdot$ time $^{-1}$). In very slow moving groundwater systems molecular diffusion contributes very little to the dispersion process and is not considered in this study. The transport equation (3.19) is used to solve for the spatial and temporal distribution of concentration, once the components of $D(x)$ are known

and the spatial distribution of velocity is determined. The transport equation includes two mechanisms of solute transport: convection and dispersion.

3.4.1 Convection

Convection is the process in which a dissolved substance is carried along with the fluid velocity. In equation 3.19 the second set of terms on the left-side represent convection. Convective movement is directly proportional to the velocity, which in turn is dependent on the ditribution of the hydraulic conductivity field.

3.4.2 Dispersion

Dispersion is a mixing phenomenon caused by pore-water velocity variabilities within the porous medium. It is the physical process which describes the tendency of a plume to spread out from the path that would be expected from convective movement alone and is represented by the third set of terms of the let side of equation 3.19.

The convection-dispersion equation (3.19) can be numerically solved to obtain the spatial and temporal distribution of concentration $c(x,t)$. The methods often used include the finite element, finite difference, and the particle tracking random walk.

Numerical dispersion is an inherent problem in the finite element and finite difference methods. A measure of the numerical dispersion is the grid Peclet number, which is conservatively approximated by

$$Pe_G \approx \frac{\Delta x}{\alpha_L} \tag{3.21}$$

if molecular diffusion is ignored. When Pe_G is greater than ten, numerical dispersion appears (Huyakorn and Pinder, 1983). Kinzelbach (1988) gave an example of potential

inaccuracies when $\alpha_L/\alpha_T >> 10$. Inorder to circumvent these numerical problems the size of the REV would need to be reduced, which would increase the computer cost and storage, to impractical limits.

3.4.3 Particle Tracking Random Walk

The particle tracking random walk (PTRW) method is free from numerical dispersion (Kinzelbach, 1988). Another advantage of the PTRW is that concentration distributions only need to be calculated when it is of interest, instead of at every time step. However, this method does not predict point concentration values as accurately as the other methods. The numerical scheme used in this study is based on the techniques described by Prickett et al (1981).

The particle tracking random walk method represents an injected mass as a large collection of particles among which the mass is divided equally. At each time step every particle is moved by a convective displacement and a dispersive displacement. The convective step is deterministic and moves particles in the direction of the pore-water velocity at that point. The dispersive step is random and is based on the physical process of dispersion. At the end of each time step the position of each particle is known, so that the average plume statistics may be calculated. The statistics are collected at certain time intervals so that the time rate of change of these statistics may be analyzed. Once a particle exits the domain, it is no longer transported and the total mass in the domain is reduced proportionally.

A brief mathematical description of the PTRW method follows. Let $x^p(t)$ represent the position of the $p-th$ particle at time t. In each time step Δt, the particle is transported

a convective displacement, Δx_c^p, and a dispersive displacement, Δx_d^p

$$x^p(t + \Delta t) = x^p(t) + \Delta x_c^p + \Delta x_d^p \tag{3.22}$$

The deterministic convective displacement is a funcitonof the velocity at $x^p(t)$, $v(x^p(t))$, and the gradient of the dispersion tensor at $x^p(t)$

$$\Delta x_c^p = [v(x^p(t)) + \nabla \cdot D(x^p(t))] \cdot \Delta t \tag{3.23}$$

The gradient terms in 3.23 are important near stagnation points. If these terms are neglected an unphysical buildup of particles may occur in regions of low hydraulic conductivity (Kinzelbach, 1988). The random dispersive displacement in each time step is, in two dimensions,

$$\Delta x_d^p = [2\alpha_L v_1(x^p(t)) \cdot \Delta t]^{1/2} \cdot z_1 + [2\alpha_T v_2(x^p(t)) \cdot \Delta t]^{1/2} \cdot z_2 \tag{3.24}$$

where z_1 and z_2 are two random values from a standard normal distribution.

The selection of Δt is an important choice in the PTRW simulation process. The computational expense of this method is proportional to the number of time steps. If a very small time step is used, the computational expense become prohibitive. If too large time step is used, overshoot errors may occur (Tompson and Gelhar, 1990). The cell Courant number is the ratio between the average convective displacement and the grid spacing

$$C_c = \frac{\overline{v(x)} \cdot \Delta t}{\Delta x} \tag{3.25}$$

where $\overline{v(x)}$ is the mean pore-water velocity. Use of time steps which force C_c greater than one result in overshoot problems. In this study the choice of Δt will be made such that $C_c < 1$.

In the PTRW method the total solute mass is represented by a hypothetical group of particles. By increasing the number of particles the solution of 3.19 becomes more consistent and reliable, but the computational expenses will increase proportionally. Though point concentration predictions become much more accurate with a larger number of particles, the accuracy of the overall plume behaviour does not increase to the same degree. Since average plume behavior is of interest in this study the total mass will be divided into 10,000 particles. The point of injection of the particles (contaminant) is given at any point within the domain and this is taken as the initial condition.

Chapter 4

RESULTS AND DISCUSSION

In this chapter the problem formulation for numerical simulations is defined, method of analysis is discussed, and the results are presented. The concepts developed in the previous sections are incorporated into a large-scale heterogeneous flow system in order to investigate the effects of variability in hydraulic conductivity field on flow and contaminant transport. A total of ten Monte Carlo simulations are performed for the case of conservative solute transport in a steady state saturated flow system.

The concentration plume, breakthrough curves and the correlation structures of the hydraulic conductivity, velocity and concentration field are obtained and analyzed. A comparative study with the traditional turning band approach is also made in order to study the effect of bimodal distribution of hydraulic conductivity field with the unimodal distribution, on the contaminant migration and the correlation structures.

4.1 Physical Domain

The domain shown in Figure 2.3 was discretized into a regular grid of 158,661 nodes with 51 nodes in each of the horizontal dimensions (x and y), and 61 nodes in the vertical dimension (z). Node spacing was 120 m in the x and y directions and 10 m in the z direction. This volume domain covers primarily the volcanic section, however portions of alluvium and paleozoic rock were also included in the problem domain due to the variable depths of the units.

4.2 Generation of Indicator Map

As discussed earlier, resistivity was used as the subsurface attribute to indicate the presence of welded tuff verses nonwelded tuff unit. The whole range of resistivity values were divided into two classes, such that the densely-welded and non-welded tuff units could be differentiated. For this purpose a threshold value of 300 ohm-m^2/m was used. The indicator coding as described previously was performed. The value at each measured data point was transformed to an indicator class based on the class in which it falls: zero if below the threshold, one if above the threshold. Resistivity logs from 24 wells were utilized. To reduce the amount of redundant data for subsequent analysis, the continuous logs were sampled at an interval of approximately 1 m. Each log then had an average of 508 resistivity measurements. An example of how the data in a typical resistivity log are transformed into the two classes is shown in Figure 4.1. The shaded areas in the figure indicate where resistivity is above the threshold value (300 ohm-m^2/m). Note that welded tuffs (the upper class) appear to represent only a portion of the welded-tuff aquifer.

Then the indicator variogram analysis was conducted and the semivariograms were

calculated for the vertical and horizontal (omnidirectional) directions using the GSLIB geostatistical software library (Deutsch and Journel, 1992) and are presented in Figure 4.2. Spherical theoretical semivariogram models were selected to represent both experimental semivariograms. Spherical semivariogram model is defined as

$$\gamma(h) = c \cdot Sph\left(\frac{h}{a}\right) \begin{array}{ll} = c \cdot \left[1.5\frac{h}{a} - 0.5\frac{h}{a}^3\right], & \text{if } h \leq a \\ = c & \text{if } h \geq a \end{array} \tag{4.1}$$

where c is the sill value, a is the range and h is the lag value. Figure 4.2 (a), shows the vertical calculated variogram values along with the fitted spherical model. It displays a nugget effect of 0.04 m, and the variogram values increase till a lag distance of 200 m, and then starts dropping down. A value of 160 m is chosen as the range at which the correlation ceases. Similarly the horizontal calculated variogram along with the fitted model is presented in Figure 4.2 (b). This variogram has a nugget effect of 0.06 m and 650 m is chosen as the range at which the correlation becomes negligible. This observation of larger horizontal correlation compares with the observed data distribution and hydrogeological setting.

The ISIM3D (Gomez-Hernandez and Srivastava, 1990) software was then used to generate the three-dimensional indicator volume data based on the selected threshold. A three-dimensional perspective of one equiprobable realization of the subsurface map of welded and non-welded tuffs is shown in Figure 4.3. The geologic heterogeneity that is expected within natural geologic formations is clearly evident in this map. Some degree of connectivity of the tuff units is apparent, although it should be pointed out that this figure represents the simulated conditions on the outer edges of the domain, where known conditioning data are sparse. More useful information can be obtained by looking within

within this map. Figure 4.4(a) shows one equiprobable map of a vertical cross-section at x =270,000 m through the subsurface data shown in Figure 4.3. The black areas represent the high resistivity zones that indicate the most likely locations of welded tuff units where potential flow paths might be present. Figure 4.4(b) shows the projection on this cross-section of the known indicator data from nine adjacent wells. Due to their proximity, these wells have the greatest influence on the simulation along this cross-section. Note that the influence of these known data depend on their distance away from the cross-section. The influence of the known data diminishes as this distance approaches the range of horizontal correlation expressed in the indicator covariance model. The general character of the distribution of welded tuffs is reproduced as can be seen by comparing the distribution of simulated welded tuff to the location of the welded tuff and vitric tuff aquifers in the hydrogeologic cross-section (shown in Figure 4.4 (c)); that is, the welded tuffs tend to be indicated primarily in the upper half of the volcanic section.

Vertical cross-sections through the subsurface data of Figure 4.3 showing equiprobable maps at x = 205,000, 207,000, and 208,000 m are presented in Figure 4.5. Welded tuffs are found in both isolated locations and as parts of large connected zones. Connected zones of welded tuffs extending horizontally up to approximately 1 km are indicated. Note that although areas of connected welded tuff do not appear to extend across the entire domain, the horizontal extent in the y direction, which is perpendicular to the page in this figure, may easily contribute to even larger spatial connectivity. In contrast, vertical connectivity of welded tuffs is usually no more than 200 m. This pattern, which is the consequence of the anisotropic covariance structure, illustrates the spatial anisotropy exhibited by volcanic tuff deposits (Istok et al., 1994).

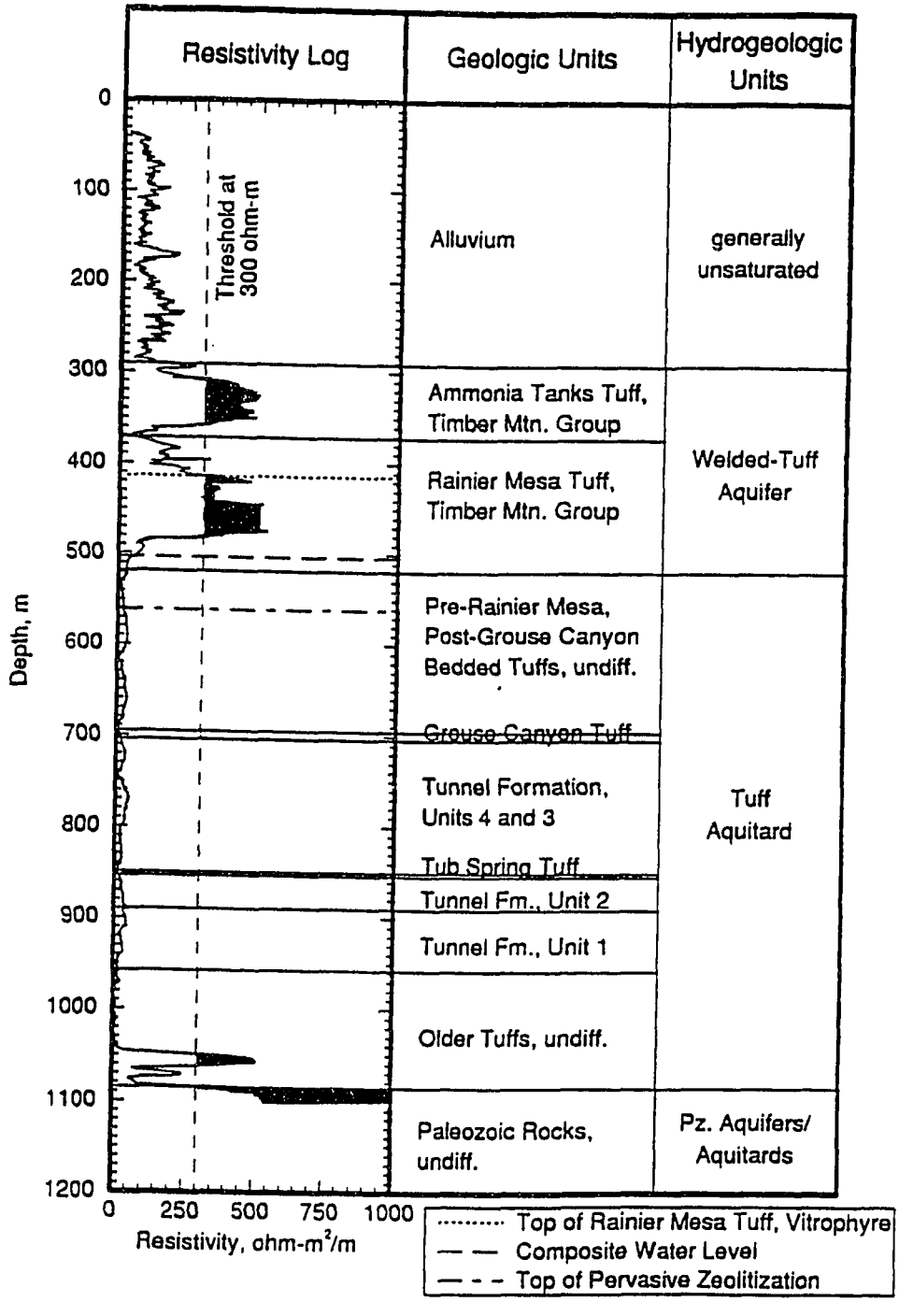

Figure 4.1: Resistivity log of well 24

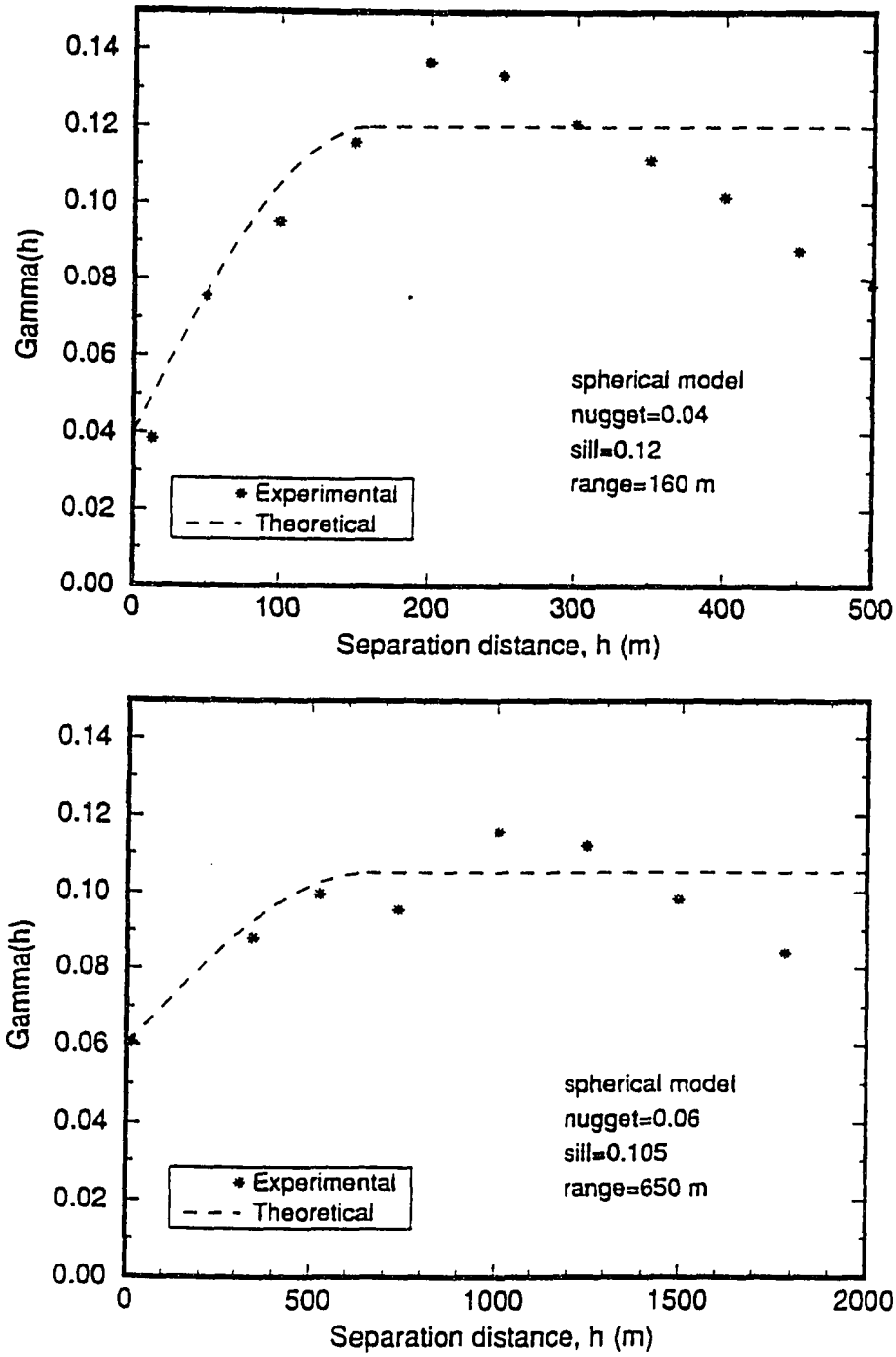

Figure 4.2: Plots of (a) vertical,and horizontal omnidirectional semivariogram of known indicator dataset

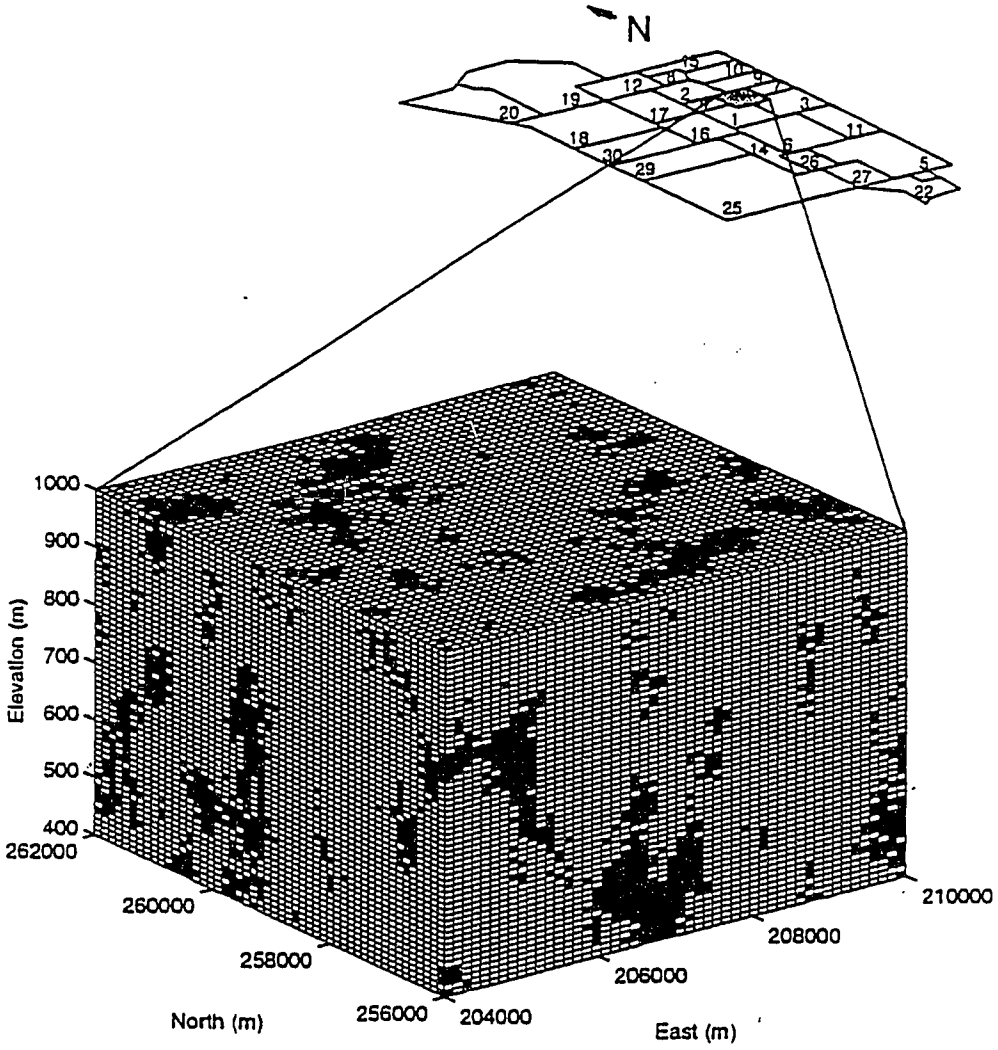

Figure 4.3: Three-dimensional perspective of the subsurface map of the volcanic section

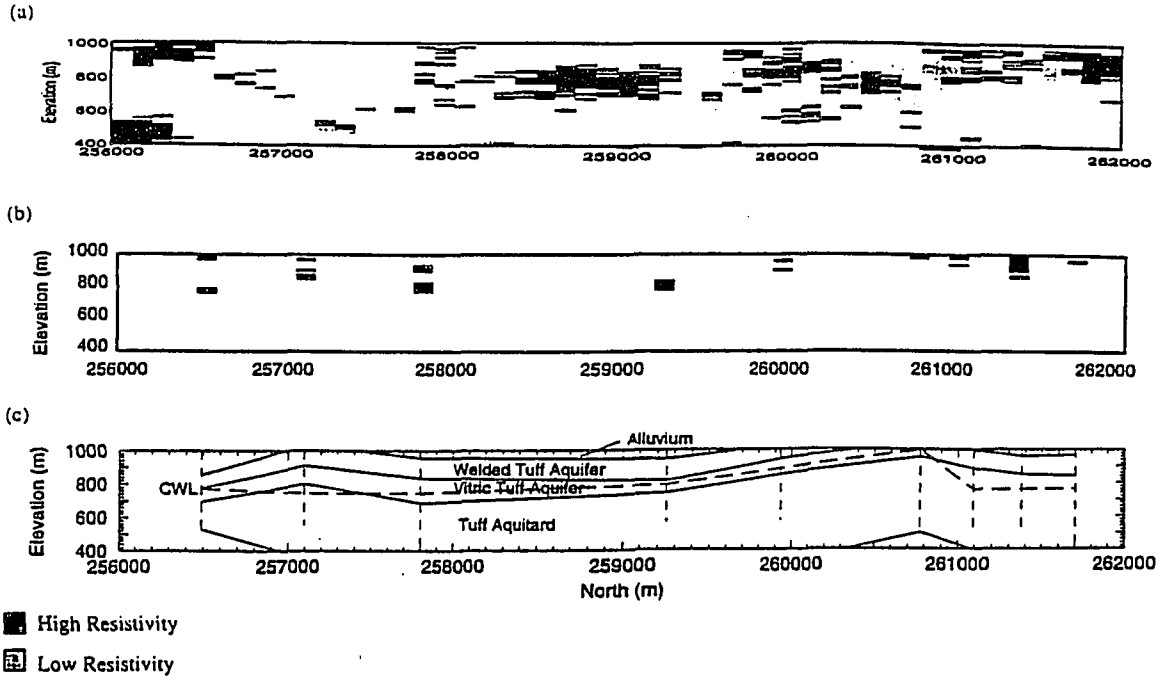

Figure 4.4: Comparison of (a)hydrogeological cross-section, (b)known indicator data from nearby wells projected on section, and (c) cross-section through simulated subsurface map

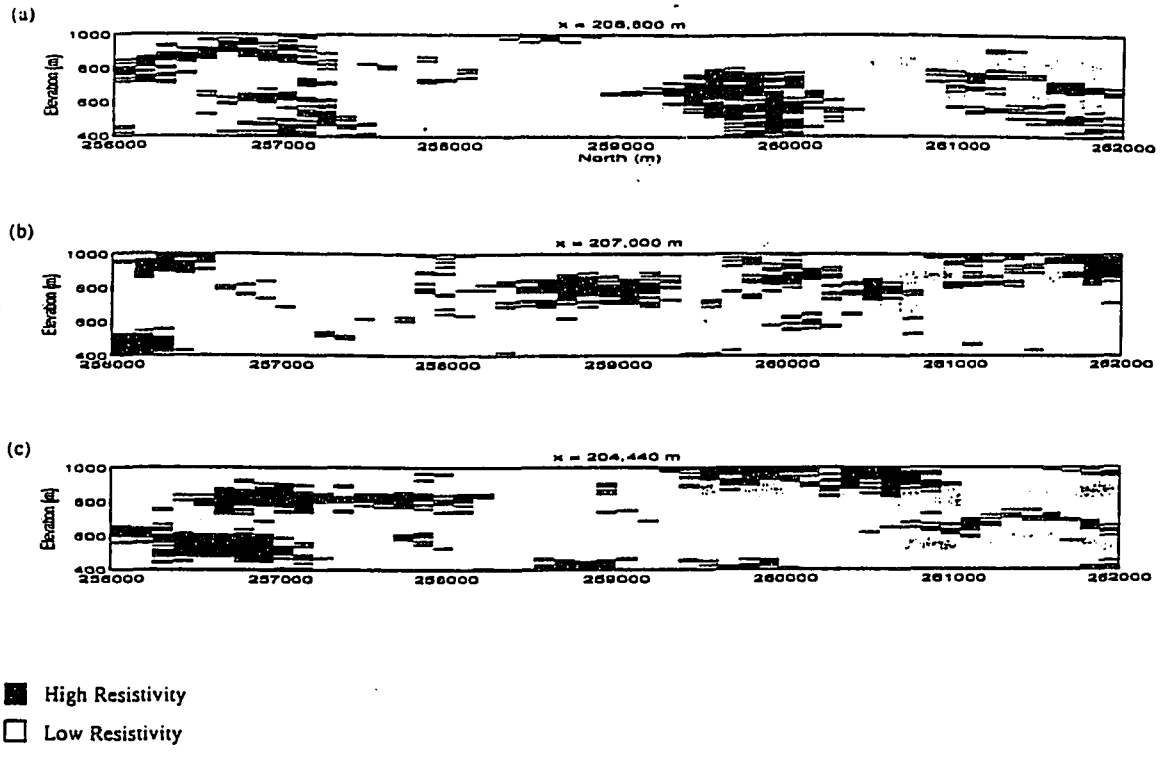

Figure 4.5: North-south cross-sections through the simulated subsurface map at (a) x =205,500 m, (b)x =207,000 m, and (c)x =208,800 m

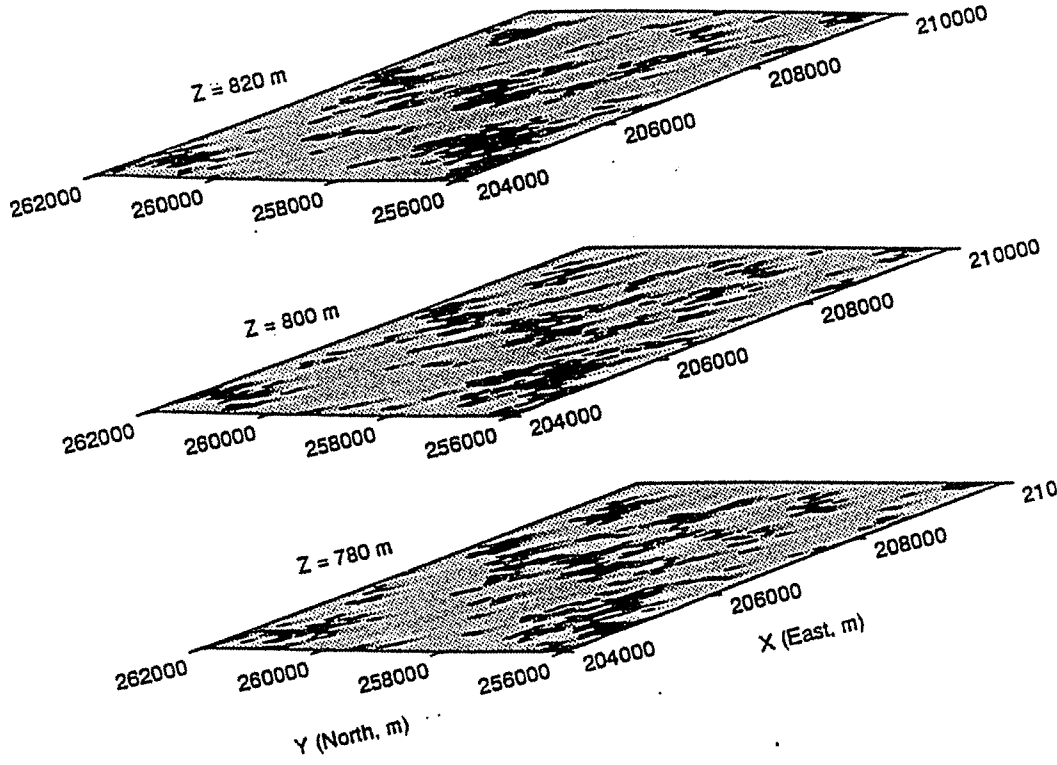

Figure 4.6: Horizontal cross-sections through the simulated subsurface map at z =780, 800, and 820 m

It is important to recognize that the two-dimensional cross-sections presented here cannot demonstrate the actual degree of three-dimensional connectivity of the welded tuff units because they cannot show the units beyond the plane of the cross-section. To help visualize the three-dimensional connectivity, horizontal cross-sections through the same equiprobable subsurface map at z =780, and 820 m are shown in Figure 4.6. To illustrate, the vertical cross-section in Figure 4.4(a), which indicates only discontinuous welded tuff between y =260,000 and 262,000 m at z =800m. In contrast, the horizontal cross-section (Figure 4.6) shows a region of nearly continuous welded tuff between y =260,000 and 262,000 m and x =207,000 and 208,000 m. Furthermore, the section at z =780 m indicates this zone of connected welded tuff extends south at least as far as y =258,000 m at this elevation. Simultaneous evaluation of multiple vertical and horizontal cross-sections within the volume data shows the increased connectivity that occurs when three dimensions are simulated in the study. Clearly, the connectivity patterns must be simulated and evaluated as three-dimensional volume data as they exist in real subsurface hydrostratigraphic units.

4.3 Generation of Hydraulic Conductivity Field

The next step was to generate hydraulic conductivity field using the soft information obtained from the resistivity values and the hard information available regarding hydraulic conductivity. The concept of Sequential Gaussian Simulation (SGS) as described in Chapter 3, was used to combine the soft and hard information. The hard information was supplied in the form of three parameters, the mean (μ), variance(σ^2) and the correlation length (λ) for both non-welded and welded tuff units, because point hydraulic conductivity values was not available. The indicator map of the resistivity values produced by the SIS simulations

and the hydraulic conductivity data are used as input into the SGS program to obtain the final hydraulic conductivity field, conditioned to both hard and soft information. As discussed in section 3.2.1, hydraulic conductivity field is log-normally distributed and the parameters used for the hydraulic conductivity field generation are presented in Table 4.1. The hydraulic conductivity field using this technique was obtained for the domain shown in Figure 2.3. The contaminant plume for this domain was observed to move very slowly over large time intervals. This necessiated in redefining the study area, as the main objective of this study was to examine the plume movement and calculate the correlation structures.

Figure 4.10, shows the new study domain, which is essentially a portion of the large domain (Figure 2.3). Also for convenience, the coordinate directions are named as x, y and z components and the x axis is assigned to the flow direction, which was observed to be from North to South at Yucca Flat. Figures 4.7, 4.8, and 4.9 shows the $x-y$, $x-z$, and $y-z$ cross-sections through one equiprobable hydraulic conductivity field. The earlier observations made regarding the indicator maps can be seen in these hydraulic conductivity maps too, especially the anisotropic covariance structure and the connectivity patterns are quite apparent. The units are better connected in the vertical direction, though the spatial continutity of these connections are small compared to the x and y directions. This may be due to the presence of large amount of conditioning data in the vertical direction.

Table 4.1: Parameters used for Hydraulic Conductivity Field generation

Nonwelded Tuff	Welded Tuff
μ = 3.15 m/yr	μ = 5840 m/yr
σ =7.81 m/yr	σ = 2464 m/yr
$\lambda_{x,y,z}$ = 60, 60, 60 m	$\lambda_{x,y,z}$ =100, 100, 60 m

4.4 Transport simulations

The domain shown in Figure 4.10 was discretized into a regular grid of 152,561 nodes with 61 nodes in x dimension, 41 nodes in y dimension and 61 nodes in z dimension. Node spacing was 20 m in x and y directions and 10 m in the z direction. The domain size was selected according to the recommendations by Ababou et al. (1988). In particular the size of the grid is much smaller than the correlation length (λ_Y) and λ_Y is much smaller than the size of the domain in order to satisfy the condition of ergodicity. All length units in the remainder of this study are meters and the time units are in years.

The hydraulic conductivity field is then used as input for the flow model, MARFLOW described in section 3.3, to solve the flow equation 3.18, to obtain the velocity field. Constant head boundaries are chosen at the left and right boundaries to produce a gradient of 10^{-3}, across the domain. The top and bottom boundaries are taken as free flow boundaries. An effective porosity value of 0.10 and 0.04 is used for non-welded and welded tuff units respectively.

The velocity field generated was then used as input to the Particle Tracking Random Walk (PTRW) code to simulate the transport of tritium. All tritium was assumed to be released instantaneously at time t_0 with a total mass of unity divided evenly between 10,000 particles. The source was assumed to be in the shape of a plate with dimensions of 20 m in the x direction, 200 m in the y direction and 100 m in the z direction. The center of the source was placed at 250 m from the upstream in the x direction to avoid the particles from going out through the upstream boundary. Microscopic dispersivity values, α_L and α_T and other parameters used for the transport simulations are listed in Table 4.2. Adsorption/desorption processes were not included in the PTRW simulations because

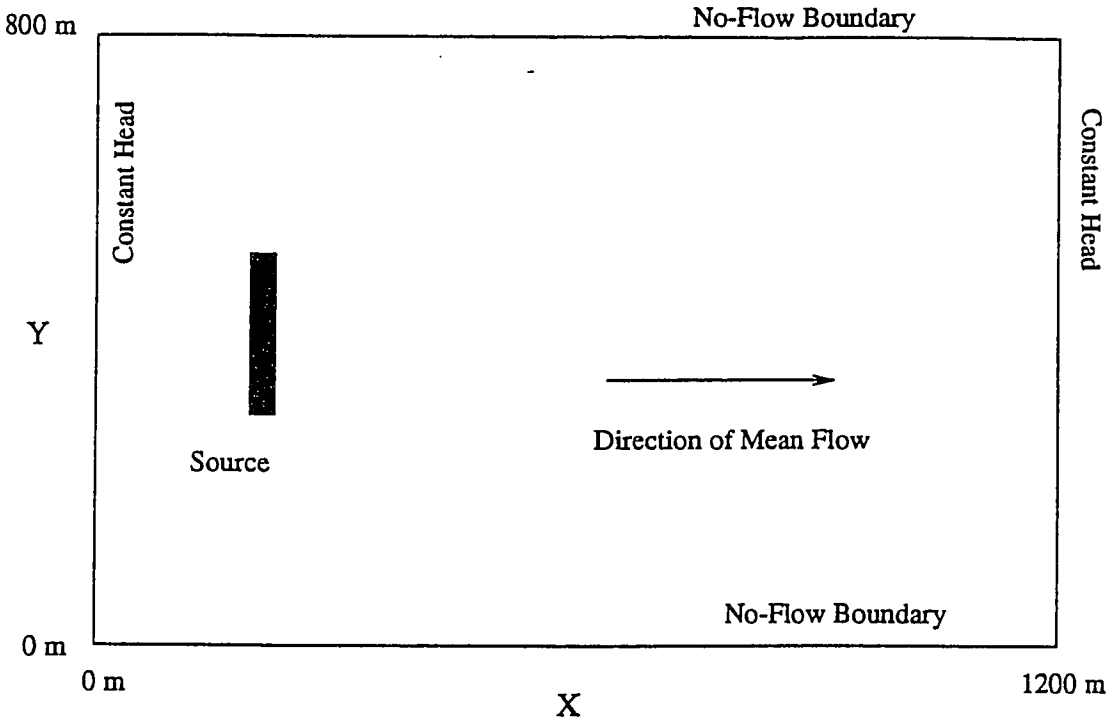

Figure 4.7: Physical domain for transport simulations

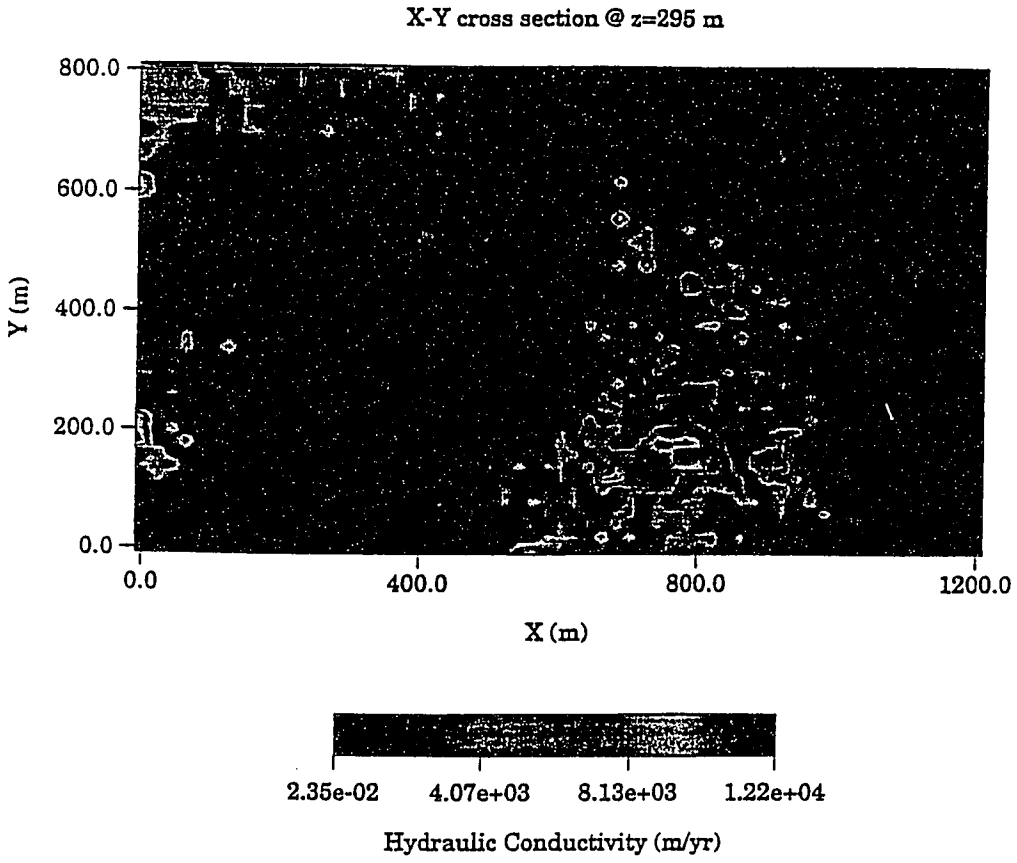

Figure 4.8: $x-y$ cross-section through the simulated hydraulic conductivity field at z =295 m

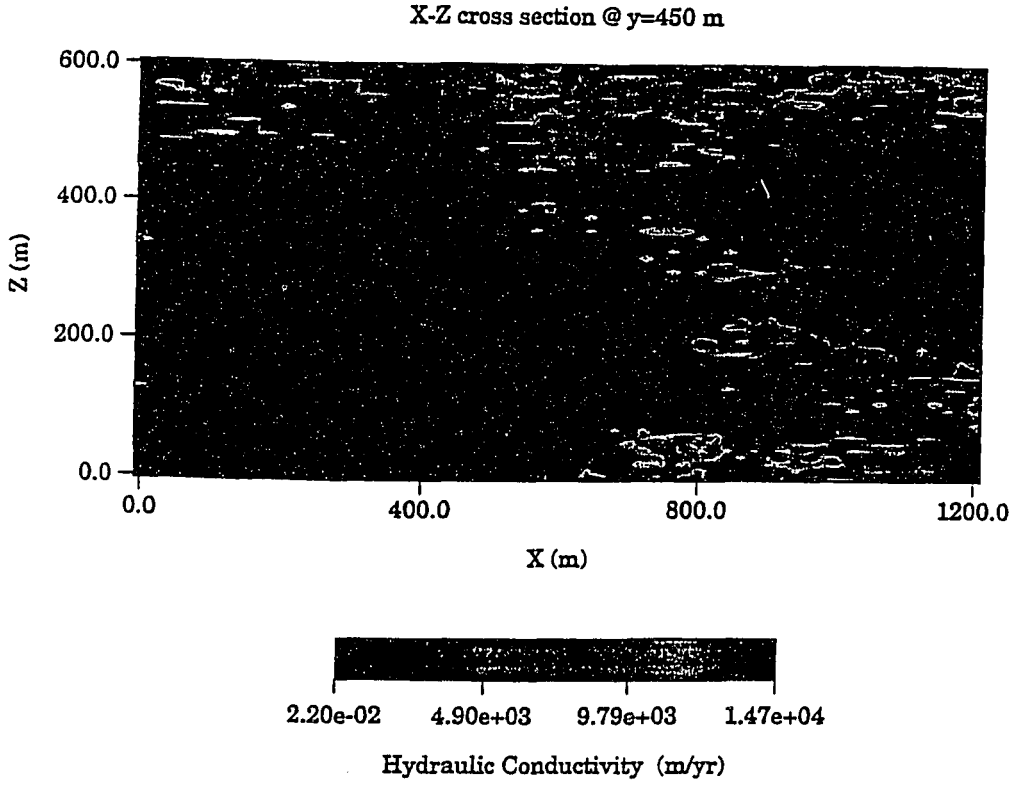

Figure 4.9: $x-z$ cross-section through the simulated hydraulic conductivity field at y =450 m

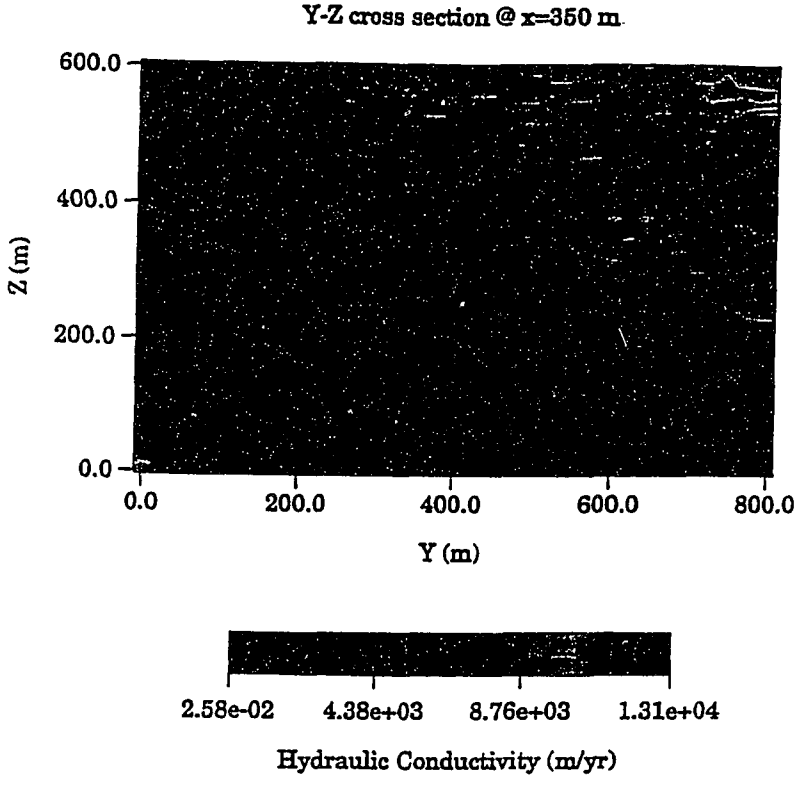

Figure 4.10: $y-z$ cross-section through the simulated hydraulic conductivity field at x =350 m

Table 4.2: Parameters used for (Particle Tracking Random Walk (PTRW) simulation

Number of particles:	10,000
α_L :	$2m$
α_T :	$0.4m$
Size of source:	20 m × 200 m × 100 m
Center of source:	250 m × 400 m × 300 m

tritium is considered non-reactive with aquifer matrix materials. All ten realizations were run for a maximum of 1000 years or until the time the particles starts leaving the domain with time-step length of five years, and radioactive decay constant for tritium of 5.6537 $\times 10^{-2}$1/yr. Figures 4.11, 4.12 and 4.13 shows the $x-y$, $x-z$ and $y-z$ cross-sections through one equiprobable normalized concentration field respectively at 1000 years. In all these figures and in the following discussion, the term normalized concentration refers to the distribution of radioactively decayed tritium, using a half-life of 12.4 years and an initial unit mass. The dominant feature of the plume as can be seen in the above mentioned figures, is the separation of small blocks of plume, travelling at different velocities. In Figure 4.11, which is the $x-y$ cross-section, the plume has a trend of moving towards the upper boundary and small blocks of plume can be seen moving separately from the main plume. Also the other interesting aspect is the presence of small block of plume near the right hand side boundary, though the major plume is concentrated at 500 m. This can be directly attributed to the presence of welded tuff units with high hydraulic conductivity values and larger spatial continuity, which in turn acts as a preferential flow path for tritium migration. This type of preferential flow path cannot be identified when the hydraulic conductivity field is generated using a single covariance structure. For this purpose, the mean (μ), variance (σ^2) and single correlation length (λ) in all three directions are obtained from the hydraulic conductivity

field generated using the bimodal distribution. These parameters are then used as input to a program implementing the Turning Band algorithm (Tompson et al, 1987), which produces the hydraulic conductivity field based on a single covariance structure. Figure 4.14 shows the $x - y$ cross-section of the normalized concentration field produced using the above mentioned hydraulic conductivity field at 20 years. One striking difference between the two concentration fields is the travel time. The single covariance based approach, overestimates the hydraulic conductivity values, for example in this case there was only 14% of welded tuff unit values with very high average hydraulic conductivity (5944 m/yr) and 86% of non-welded tuff units with very low hydraulic conductivity (2.7 m/yr). But the average value of hydraulic conductivity for unimodal distribution is 834.5 m/yr, resulting in higher hydraulic conductivity values for the whole domain, which is a clear representation of the effect due to overliers discussed in statistical literature. Also the concentration plume obtained using single covariance approach moves as whole as can be seen in Figure 4.14, without showing any effects of preferential flowpaths. The $x - z$ cross-section of the concentration field obtained using the bimodal distribution (Figure 4.12), shows an upward trend, which is a direct result of the high hydraulic conductivity values present in the top zone as can be seen in $x - z$ cross-section of the hydraulic conductivity in Figure 4.8. Also the separation of small blocks of plume can be seen here.

4.5 Breakthrough Curves

The number of particles passing a plane in the x direction as a function of time is presented as breakthrough curves. The breakthrough curve for the bimodal and unimodal distributions are presented in Figures 4.15 and 4.16 respectively. The breakthrough curve of the bimodal

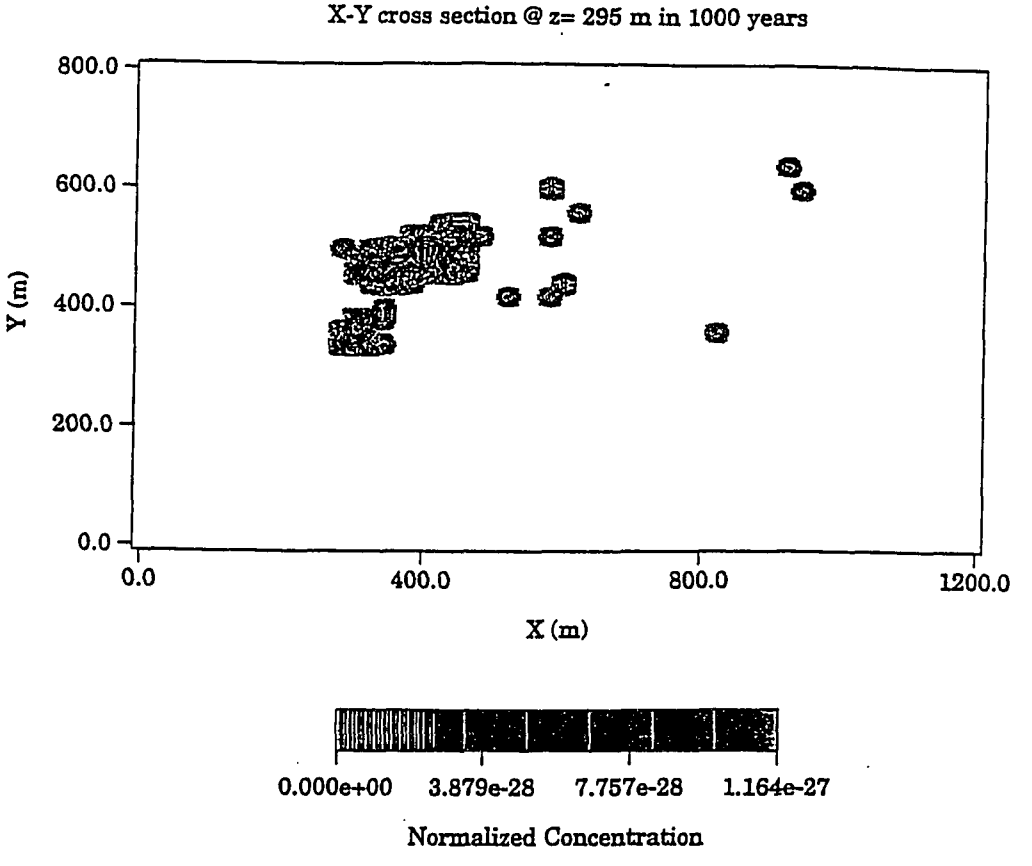

Figure 4.11: $x - y$ cross section through one equiprobable concentration field at x =295 m

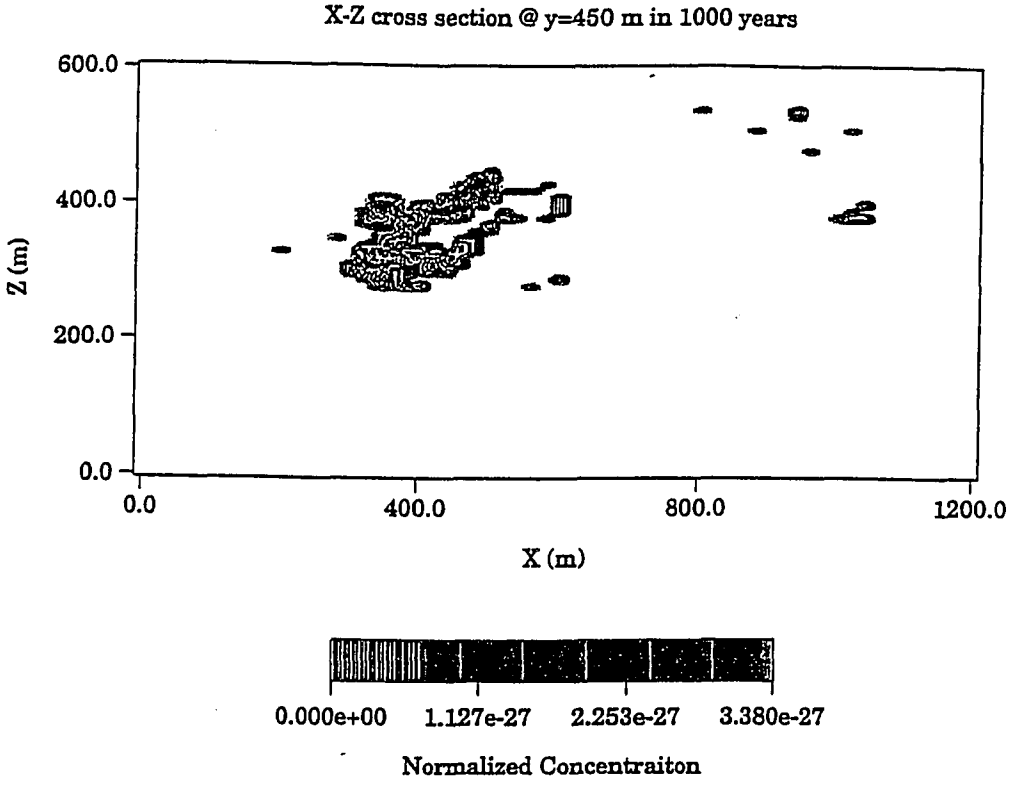

Figure 4.12: $x - z$ cross section through one equiprobable concentration field at y =450 m

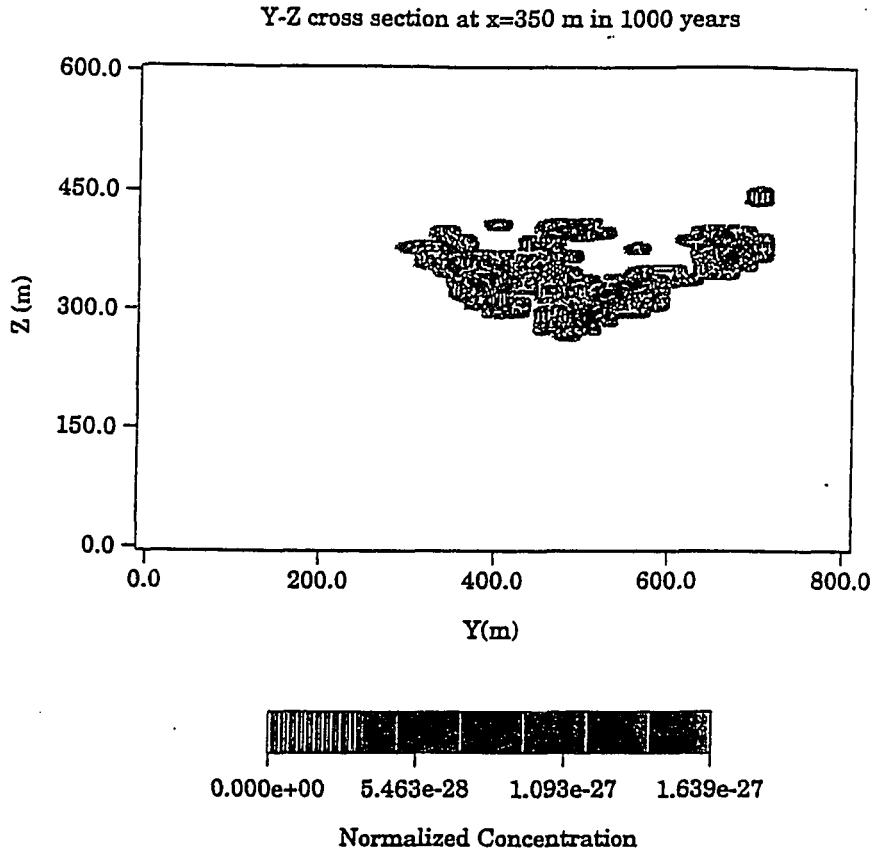

Figure 4.13: y – z cross section through one equiprobable concentration field at x =350 m

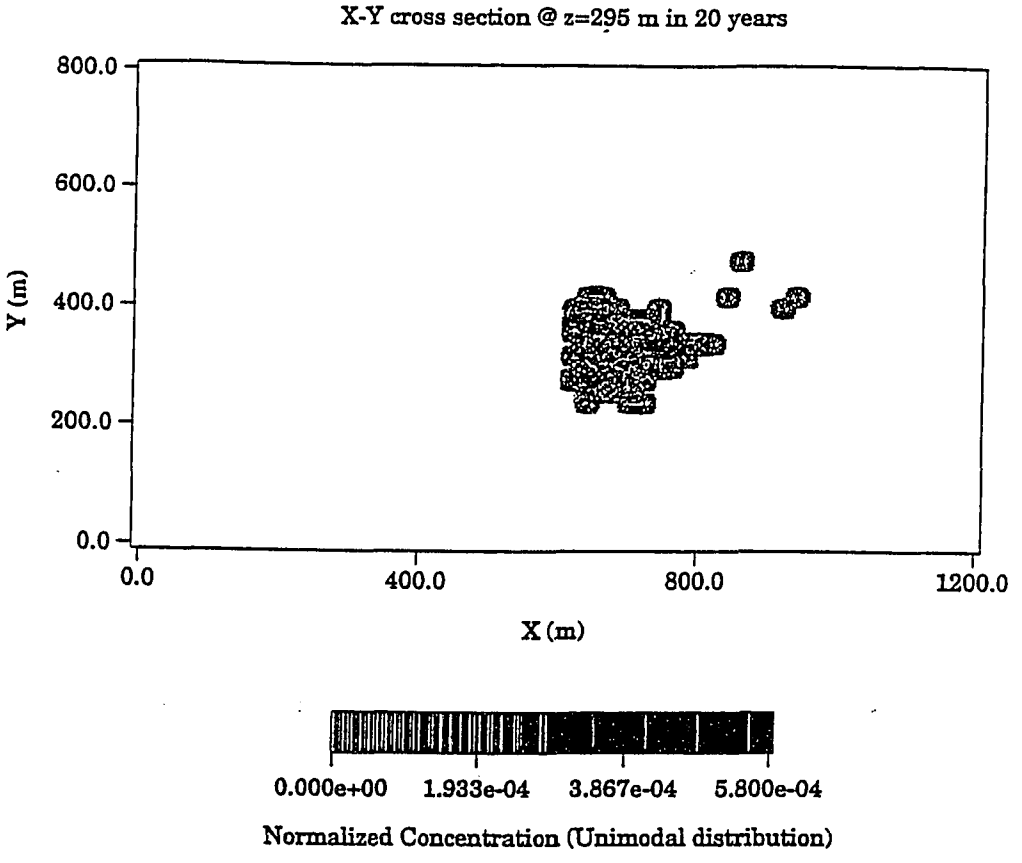

Figure 4.14: $x-y$ cross section through one equiprobable concentration field (single covariance structure) at z =295 m

distribution shows a larger tail and two peaks. The large tail is due to the fast arrival of few particles through the preferential flowpaths and the remaining particles crossing the plane at a slower rate. The breakthrough curve of the unimodal distribution has a single peak and the spread of the tail is much less compared to the bimodal distribution.

4.6 Correlation Structure

Correlation Structure characterizes the correlation between the values taken by the property at two neighboring points in space. This is a useful tool to determine the correlation of the contaminant plume in space. The correlation structures obtained at different times, is useful to study the evolution of the plume in space with time. This is of great use to optimize the monitoring network to capture the developing plume. The correlation structures of the hydraulic conductivity, velocity and concentration are presented in this section. Since concentration is a function of time, correlation structures are obtained at different times to study the behaviour of the plume.

4.6.1 Hydraulic Conductivity

The random hydraulic conductivity fields generated by the Sequential Gaussian Simulation method are analyzed to ensure that they reproduce the correlation structure assumed. The correlation structure of the hydraulic conductivity field is determined by calculating the correlation between values of $Y(x)$ at point $x_n, n = 1, 2, 3, ..., N$, where N is the number of nodes in the field. The sample mean of $Y(x)$ is

$$\mu(Y) = \frac{1}{N} \sum_{n=1}^{N} Y(x_n) \tag{4.2}$$

and the sample variance about that mean is

$$Var(Y) = \frac{1}{N}\sum_{n=1}^{N}[Y(x_n) - \mu(Y)]^2 \tag{4.3}$$

With the sample mean and variance known the correlation structure for $Y(x)$ is determined in each of the principal directions for both non-welded and welded units separately, as their correlation lengths are assumed to be different. The correlation between all points separated by r_i is

$$\rho_Y(r_i) = \frac{\frac{1}{N}\sum_{n=1}^{N}[Y(x_n) - \mu(Y)] \cdot [Y(x_n + r_i) - \mu(Y)]}{Var(Y)} \tag{4.4}$$

It follows that

$$\rho_Y(r_i = 0) = 1 \tag{4.5}$$

Once the correlation is determined for numerous separation distances the sample correlation length is equal to the separation distance at which the correlation is equal to e^{-1}. Figures 4.17, 4.18 and 4.19 shows the computed correlation structures of $lnK(x)$ in all the three directions for the non-welded tuff units respectively, along with the assumed exponential distribution. Figures 4.20, 4.21, and 4.22 are similarly the correlation structures for the welded tuff units. These figures indicate that the Sequential Gaussian Simulation method accurately reproduces the anisotropic correlation structure for both the units.

4.6.2 Velocity

The velocity field correlation structure is evaluated in the same way as $Y(x)$, except that at each point the velocity has three components. The sample mean and variance for each

of these components are determined in the same way as for $Y(x)$. In a three-dimensional problem the velocity correlation structure has nine components and can be represented in matrix form by

$$\rho_v(r) = \begin{vmatrix} \rho_{v1}(r1) & \rho_{v1}(r2) & \rho_{v1}(r3) \\ \rho_{v2}(r1) & \rho_{v2}(r2) & \rho_{v2}(r3) \\ \rho_{v3}(r1) & \rho_{v3}(r2) & \rho_{v3}(r3) \end{vmatrix} \tag{4.6}$$

Figures 4.23, 4.24 and 4.25 display the three components of the velocity correlation in the principal directions. As expected, the correlation structures display anisotropy and the velocities in the transverse directions exhibit hole effects. By definition the hole effect occurs when the spatial correlation between two points become negative. A velocity field hole-effect signifies a velocity field which periodically repeats itself with clusters of large and low values.

4.6.3 Concentration

The calculation of the correlation strucutures for the concentration field is little different than those explained above. This is because the concentration field is time-dependent and non-stationary. Stationarity is one of the assumptions for variogram analysis or for obtaining the correlation function. In other words, the concentration field has spatial trend, which is an indication of the presence of more than one statistical population (strata) with significantly different mean concentrations. Directly using the concentration field for obtaining the correlation functions can result in inaccurate correlation lengths. The trend present in the concentration values needs to be removed in order to calculate the correlation function. This can be done by identifying the different distributions present in the concentration field and then subtracting the respective means from the corresponding populations. The

dtrended concentration field will satisfy the constant mean assumption, and then the correlation function can be calculated using these values. The different statistical distributions present are identified with the help of a lognormal probability plot of the concentration values (Singh etal, 1994). Figure 4.26 shows a lognormal probability plot of the concentration field at a specific time. The whole range of values are divided into three different populations based on the change of slopes as shown in the figure. The cutoff values are calculated and then the respective mean for each population is calculated and subtracted to obtain a dtrended concentration field.

Since the concentration field is time-dependent, the correlation function is calculated at ten different time steps for all the ten realizations. The largest possible time is selected in order to allow the plume to spread out sufficiently, yet small enough to still have all the particles in the domain. Figures 4.27, 4.28, and 4.29 shows the correlation functions of the concentration field at 1000 years for one realization in all the three principal directions respectively. The correlation lengths in x, y and z directions are 38.67, 108.65, and 75.0 m respectively. The correlation length is larger in the y direction, than the x direction indicating that the distribution of concentration is more spatially continuous in the y direction than the x direction. This may be because of the shape of the source, which is in the shape of a plate. The correlation length in the z direction is also larger than the x direction, again indicating larger spread in the z direction. The correlation function in all the three directions display a trend, or non-stationarity. Figures 4.30, 4.31, and 4.32, shows the correlation function of the concentration field obtained using the unimodal hydraulic conductivity field. In this case, the correlation lengths in both x and y directions have higher values indicating larger spatial continuity, but the correlation length in the z direction is much smaller than

the value obtained for bimodal distribution, indicating very less plume spreading in the z direction. Also in this case, only y and z directions display hole effect, unlike the bimodal distribution, in which all the three directions display a trend indicating non-stationarity, which can be directly attributed to the fluctuations in the concentration values due to the presence of two different populations.

In order to study the behaviour of the correlation function with time, the correlation lengths are determined at ten different time intervals. Figures 4.33, 4.34 and 4.35 shows the correlation lengths obtained for one particular realization in all the three prinicipal directions In general, the correlation lengths seems to increase with time, reflecting the increase of spatial continuity of the plume with time. But the rate of increase is much higher in the y and z directions, again indicating larger spreading in both these directions. The correlation lengths for the concentration field using the unimodal distribution of hydraulic conductivity is presented in Figures 4.36, 4.37 and 4.38 for the three principal directions respectively. As said earlier, the value of the correlation lengths are higher in this case, suggesting higher spatial continuity of the plume. In this case also, the correlation length increased with time, again reflecting larger spatial continuity as time increases.

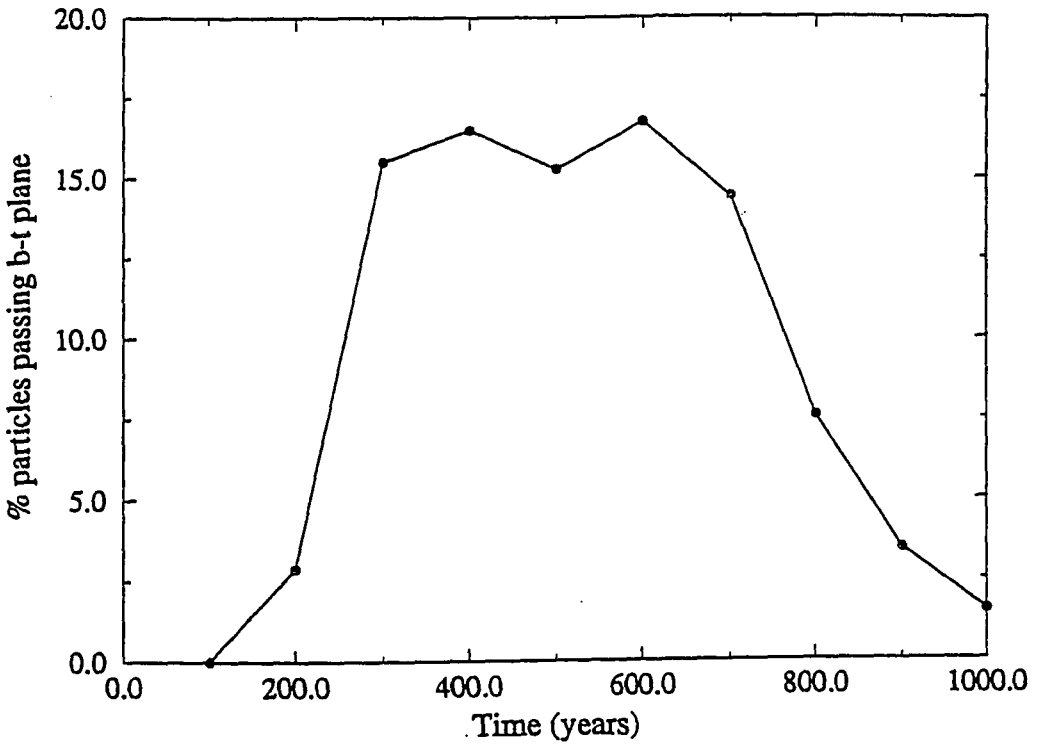

Figure 4.15: Breakthrough Curve for Bimodal Distribution

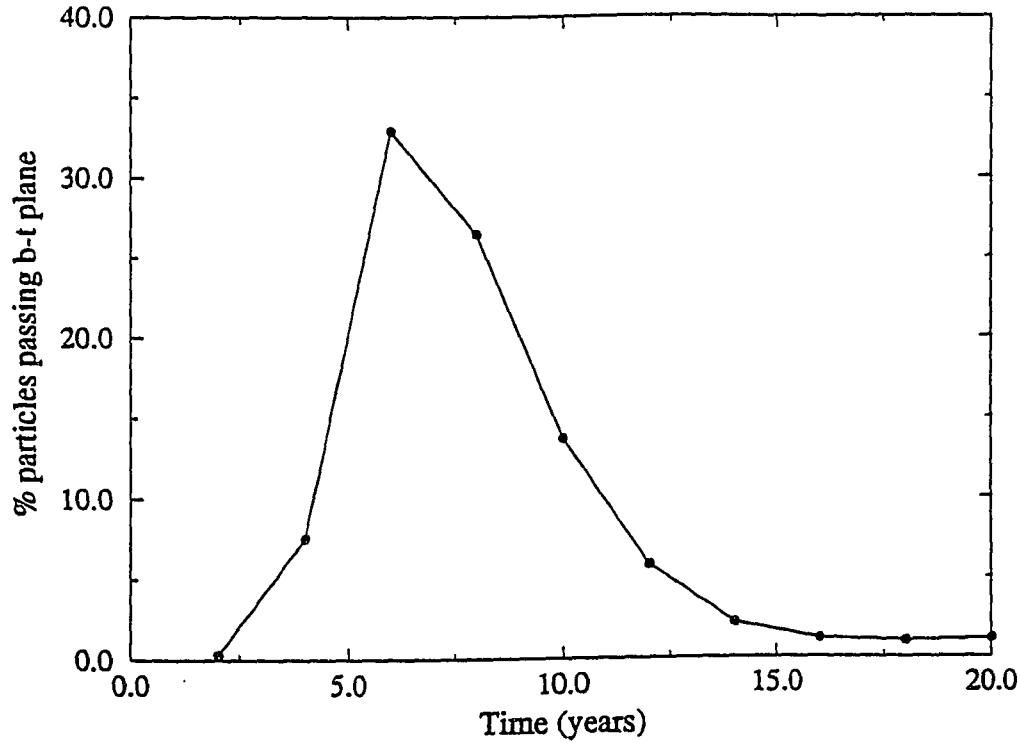

Figure 4.16: Breakthrough Curve for unimodal Distribution

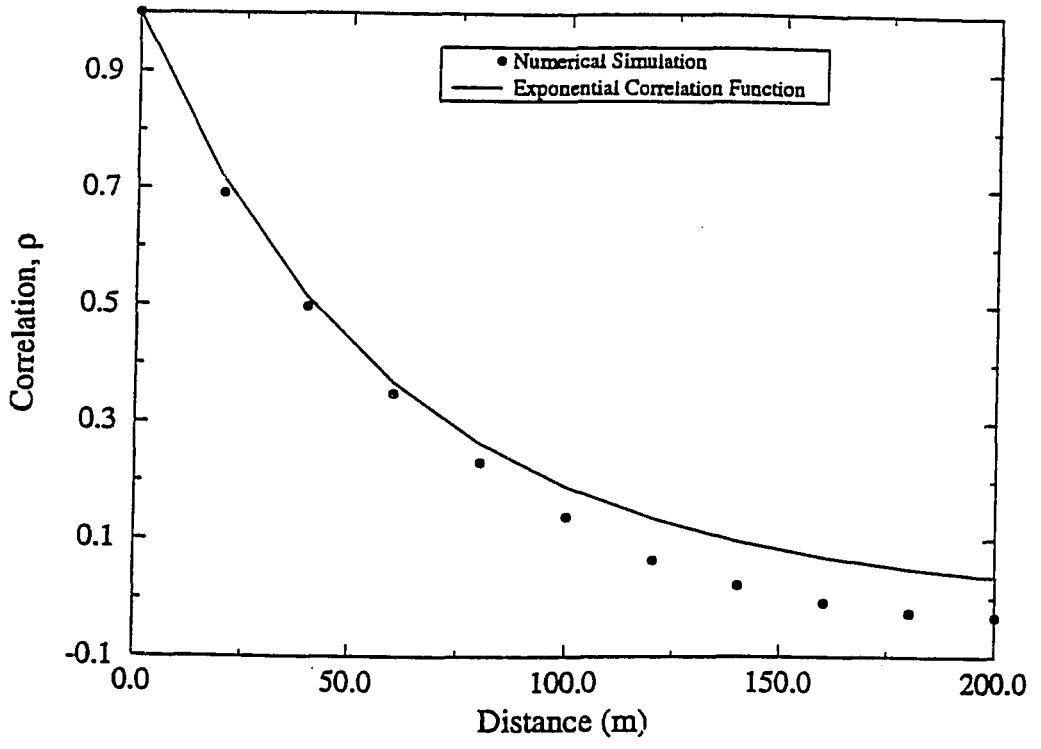

Figure 4.17: Correlation structure of lnK in the x direction along with the assumed exponential correlation function, (λ =60 m) for non-welded tuff

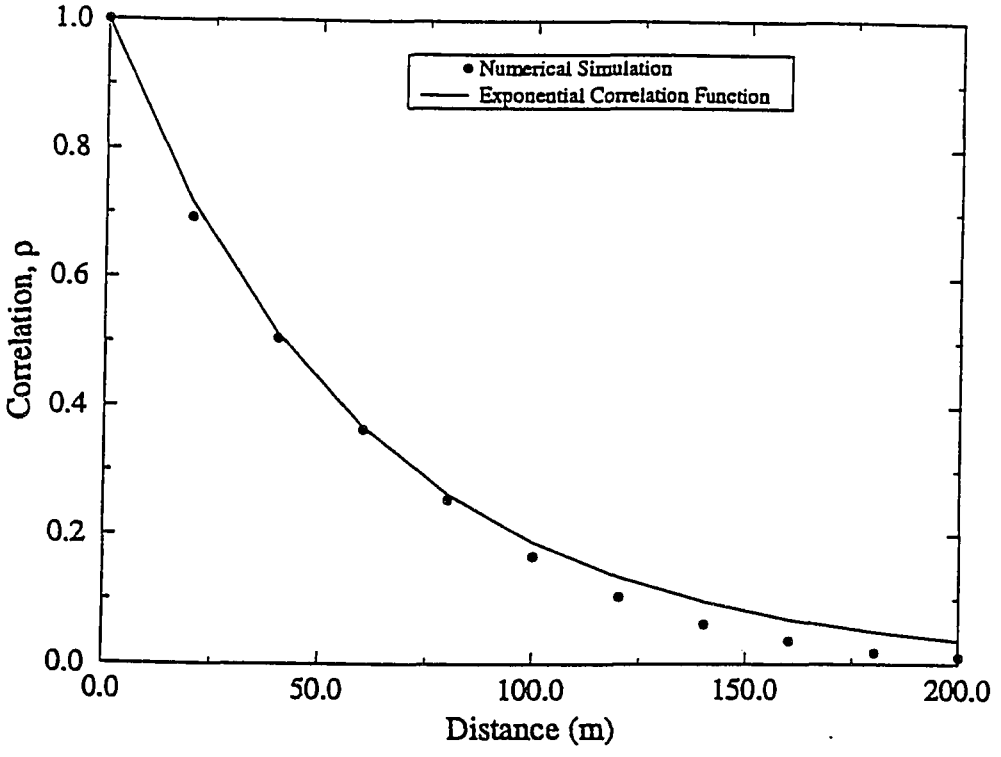

Figure 4.18: Correlation structure of lnK in the y direction along with the assumed exponential correlation function, (λ = 60 m) for non-welded tuff

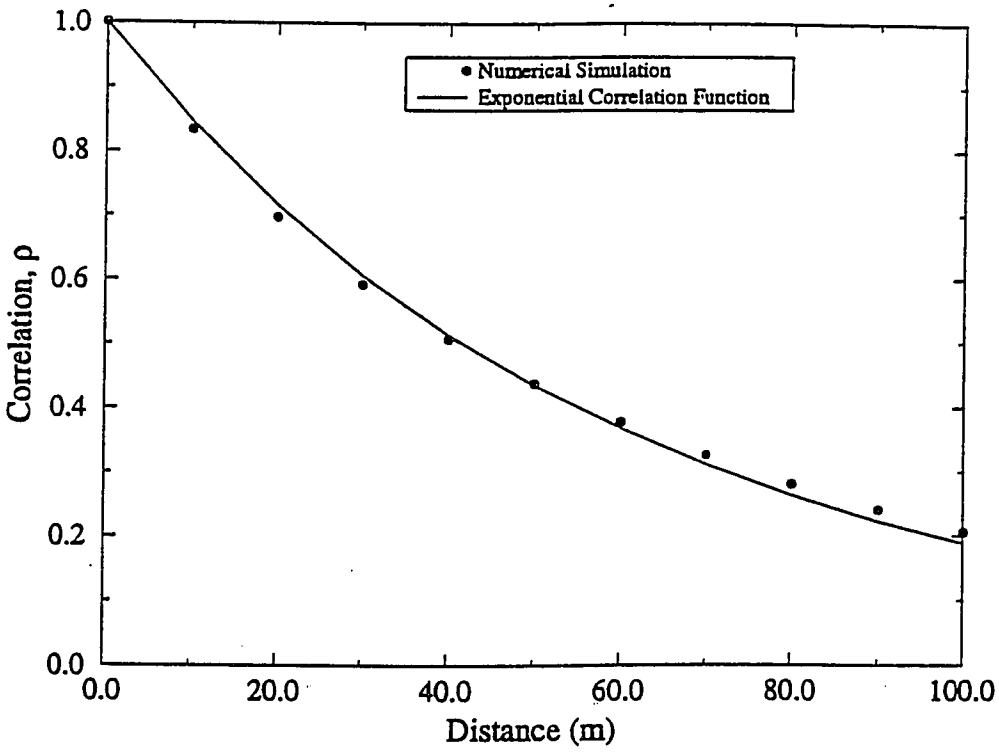

Figure 4.19: Correlation structure of lnK in the z direction along with the assumed exponential correlation function, ($\lambda = 60$ m) for non-welded tuff

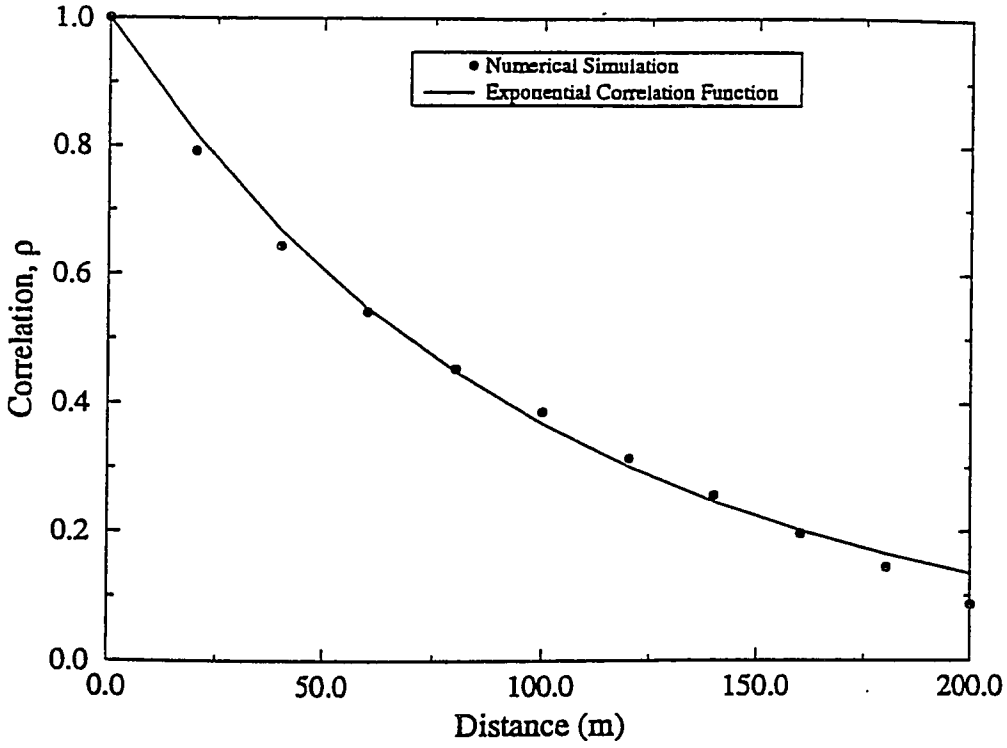

Figure 4.20: Correlation structure of lnK in the x direction along with the assumed exponential correlation function, (λ = 100 m) for welded tuff

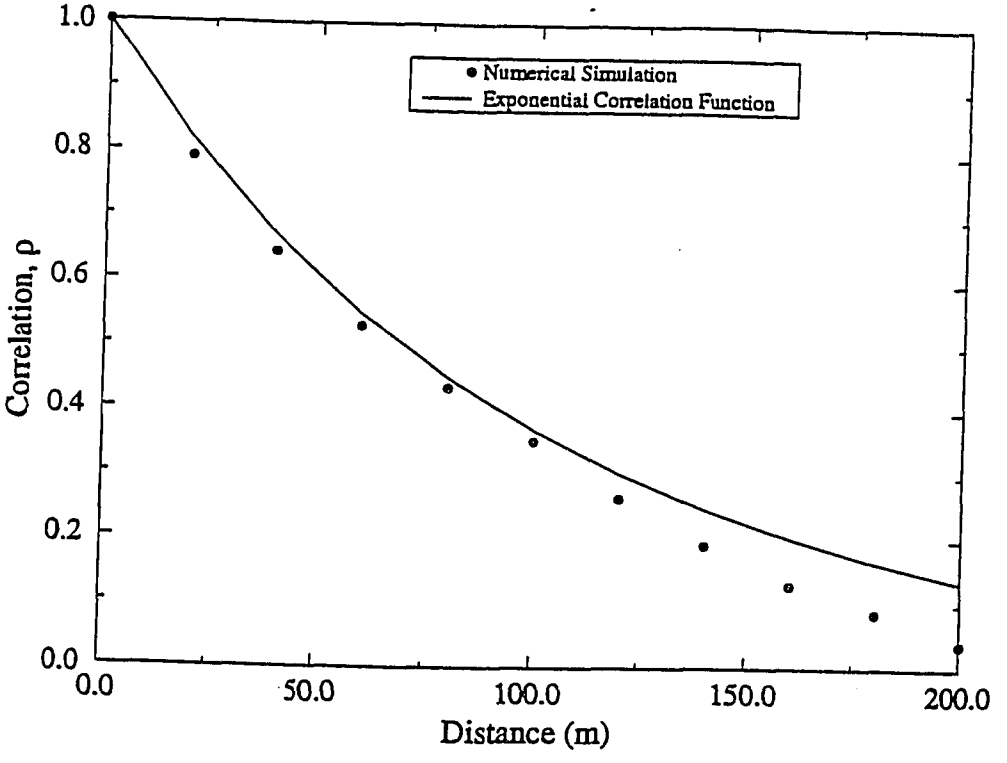

Figure 4.21: Correlation structure of lnK in the y direction along with the assumed exponential correlation function, (λ = 100 m) for welded tuff

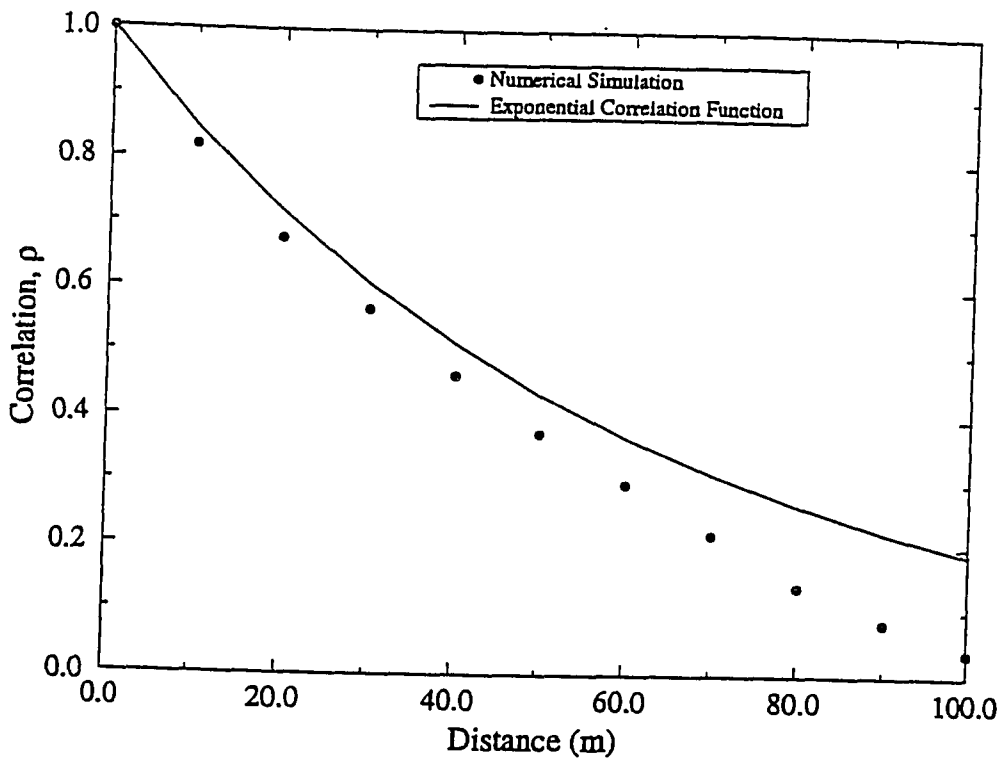

Figure 4.22: Correlation structure of lnK in the z direction along with the assumed exponential correlation function, (λ=60 m) for welded tuff

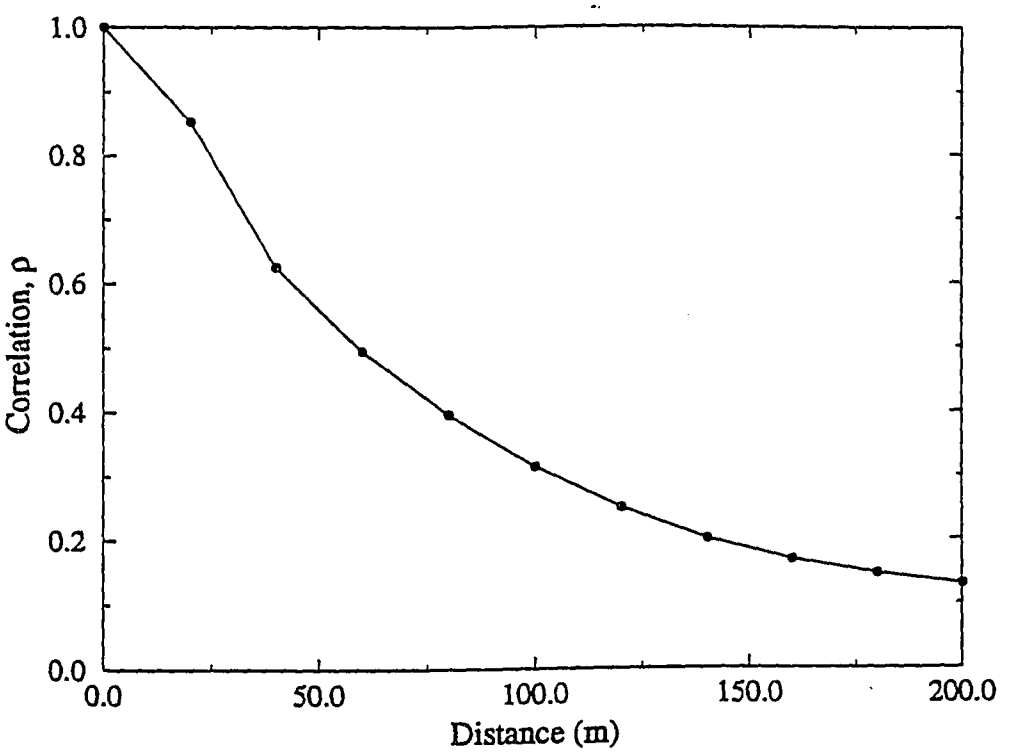

Figure 4.23: Correlation structure of the velocity field in the x direction

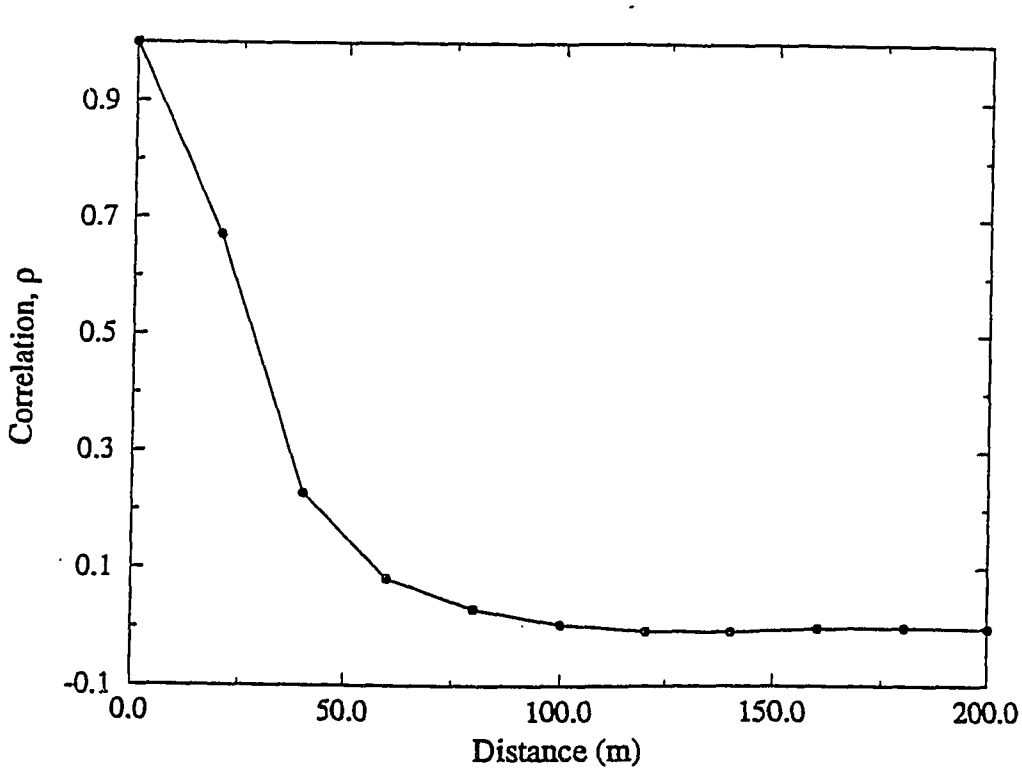

Figure 4.24: Correlation structure of the velocity field in the y direction

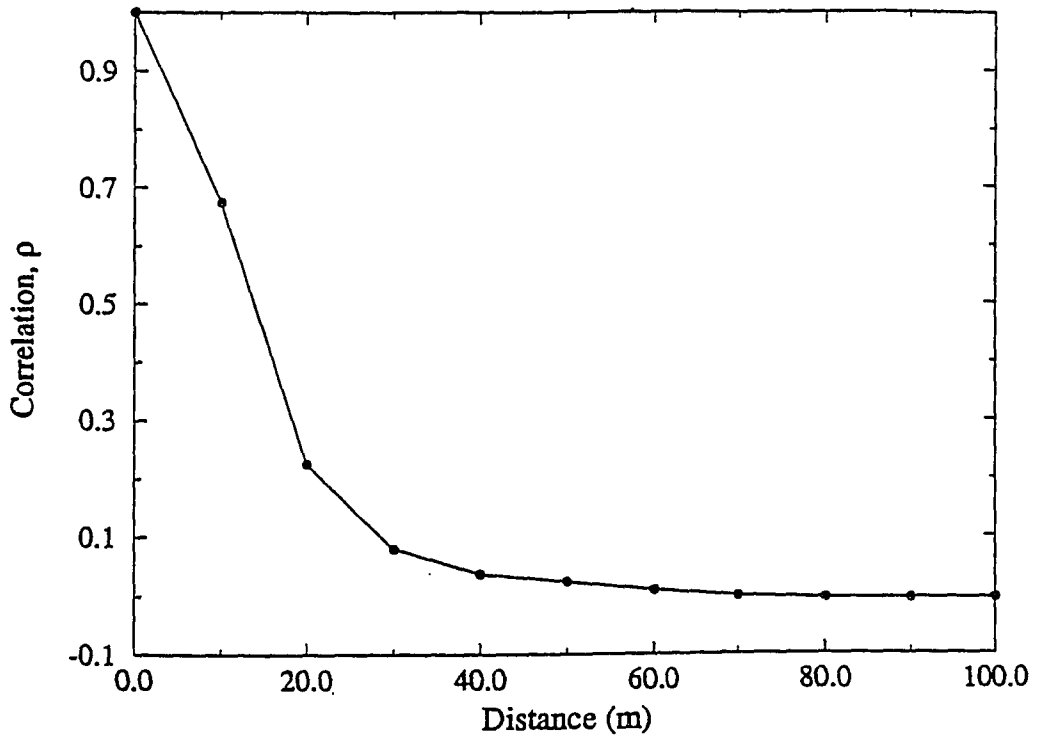

Figure 4.25: Correlation structure of the velocity field in the z direction

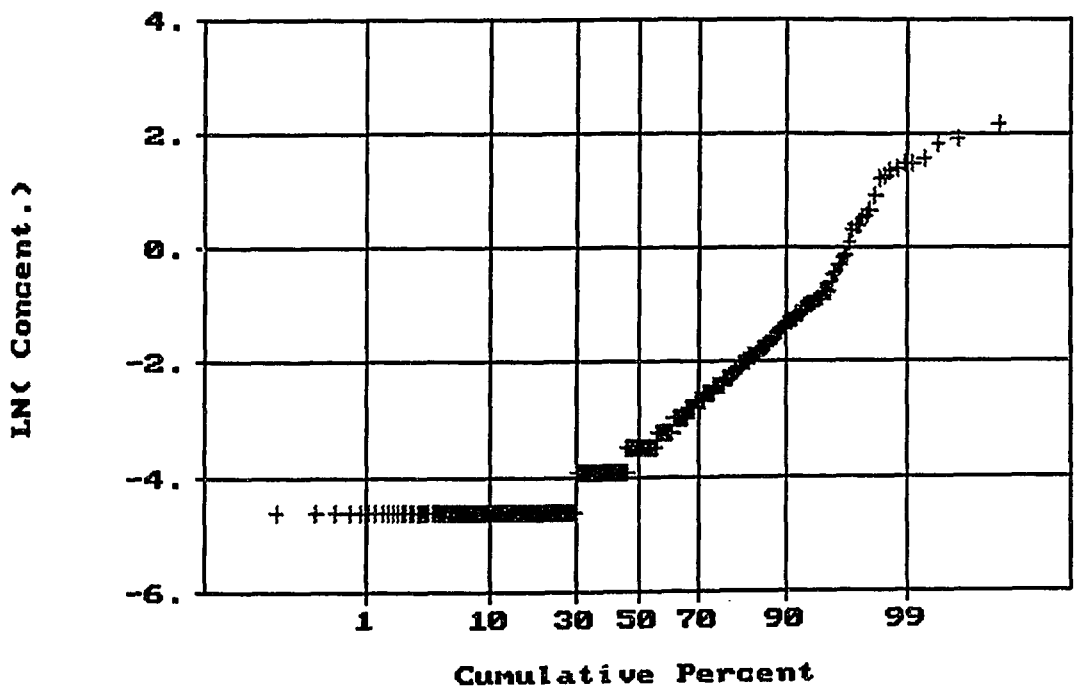

Figure 4.26: Log-normal probability plot of the concentration field at $t = 1000$ years

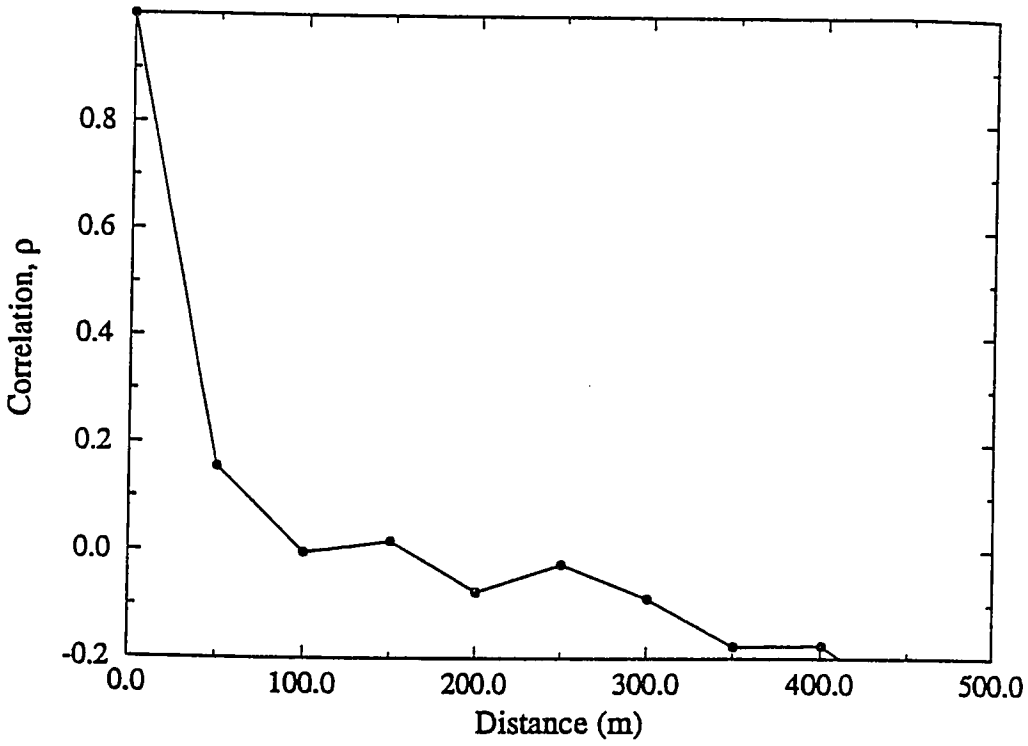

Figure 4.27: Correlation structure of the concentration field in the x direction at time, $t = 1000$ years

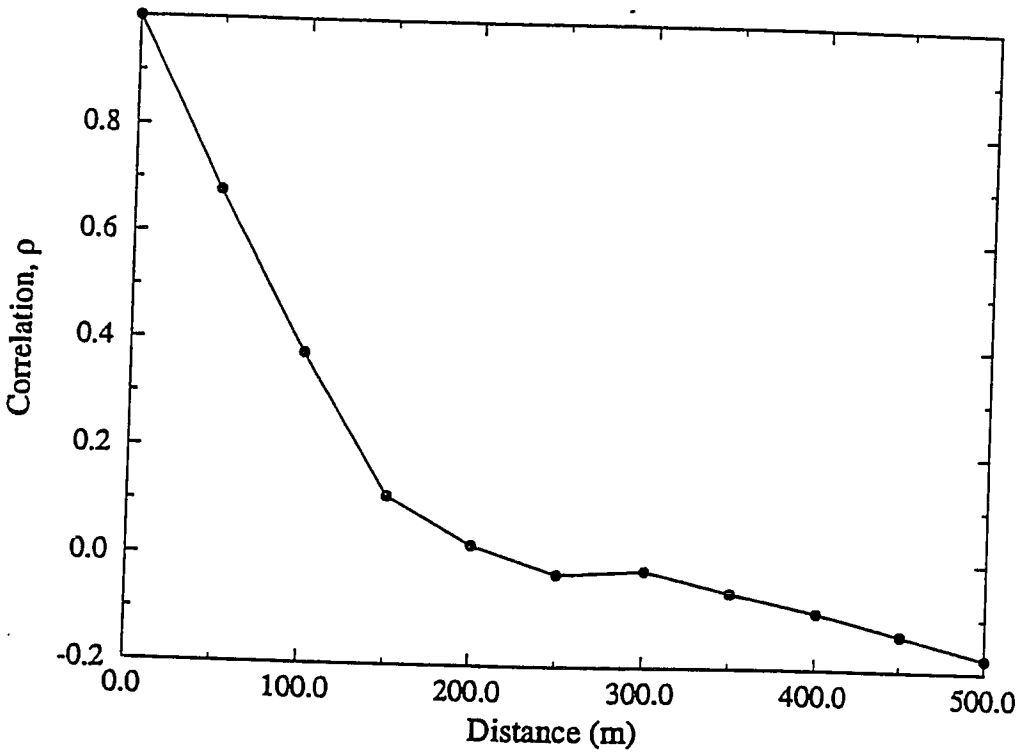

Figure 4.28: Correlation structure of the concentration field in the y direction at time, $t = 1000$ years

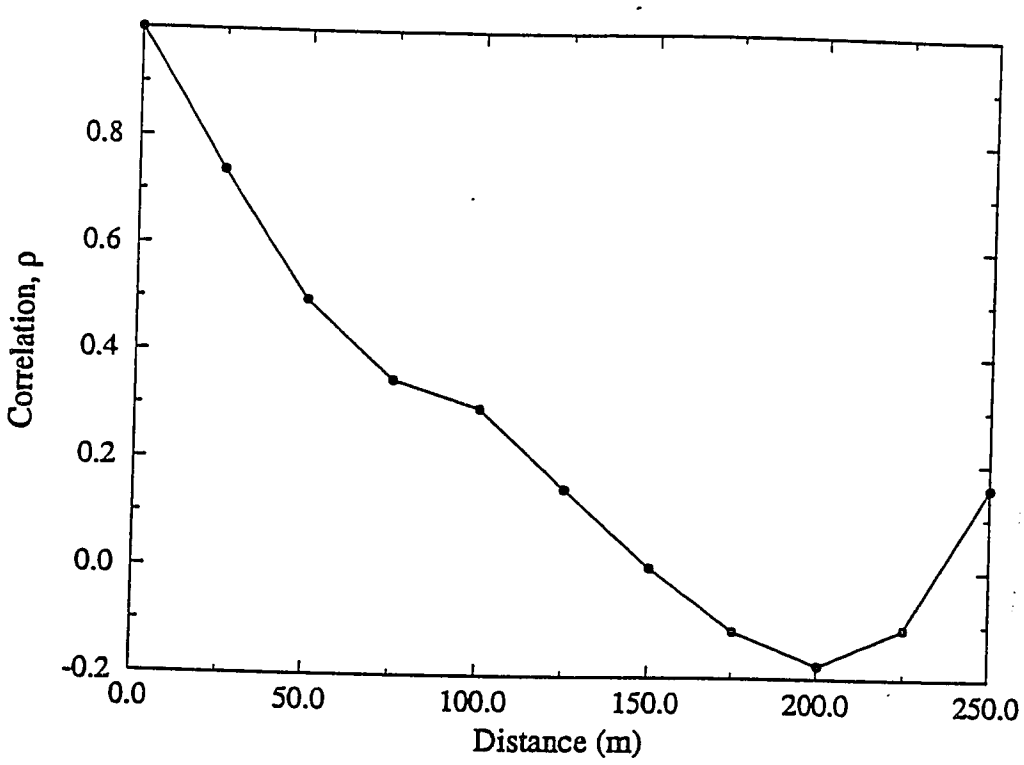

Figure 4.29: Correlation structure of the concentration field in the z direction at time, $t = 1000$ years

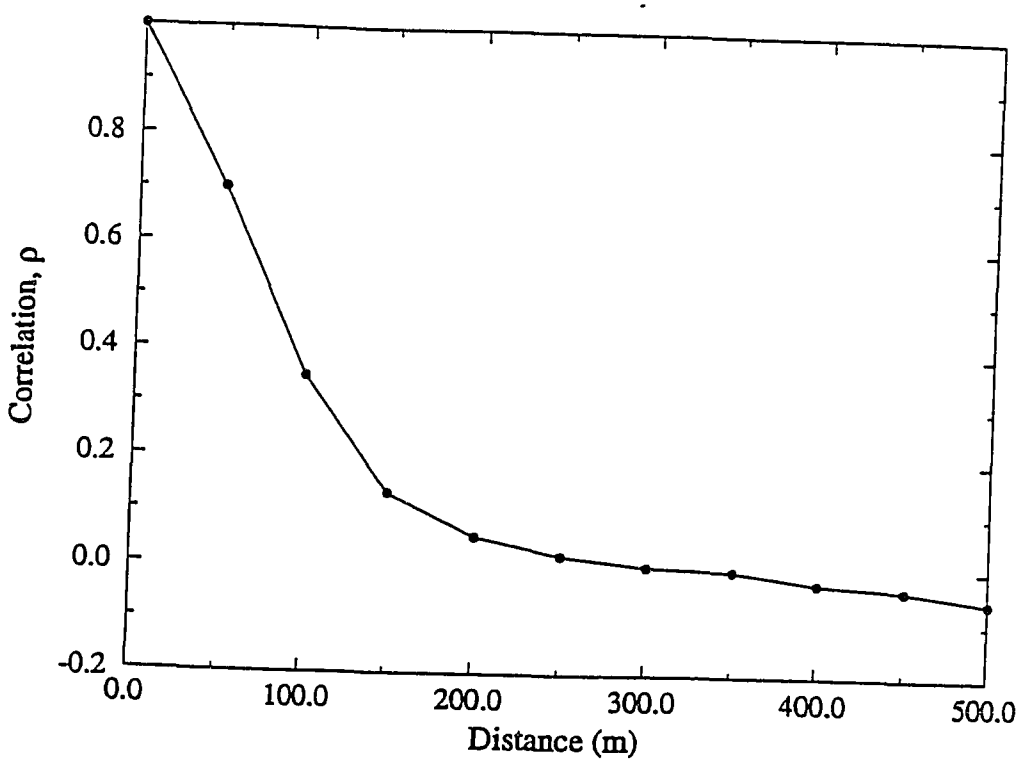

Figure 4.30: Correlation structure of the concentration field (single covariance structure) in the x direction at time, $t = 20$ years

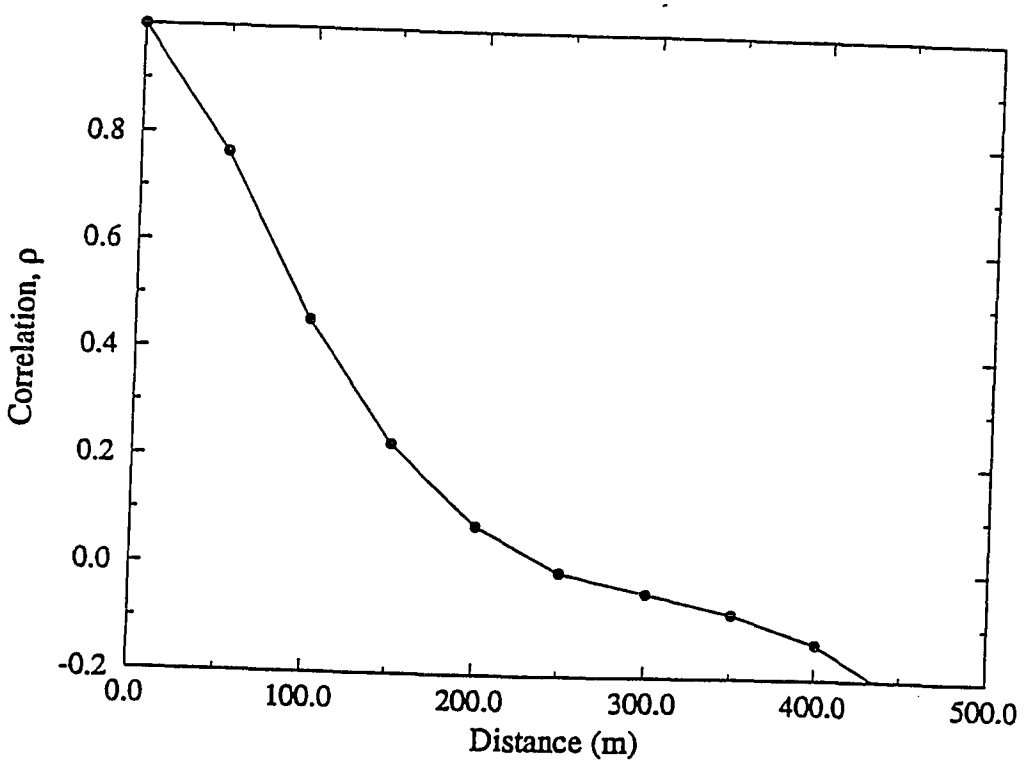

Figure 4.31: Correlation structure of the concentration field (single covariance structure) in the y direction at time, $t = 20$ years

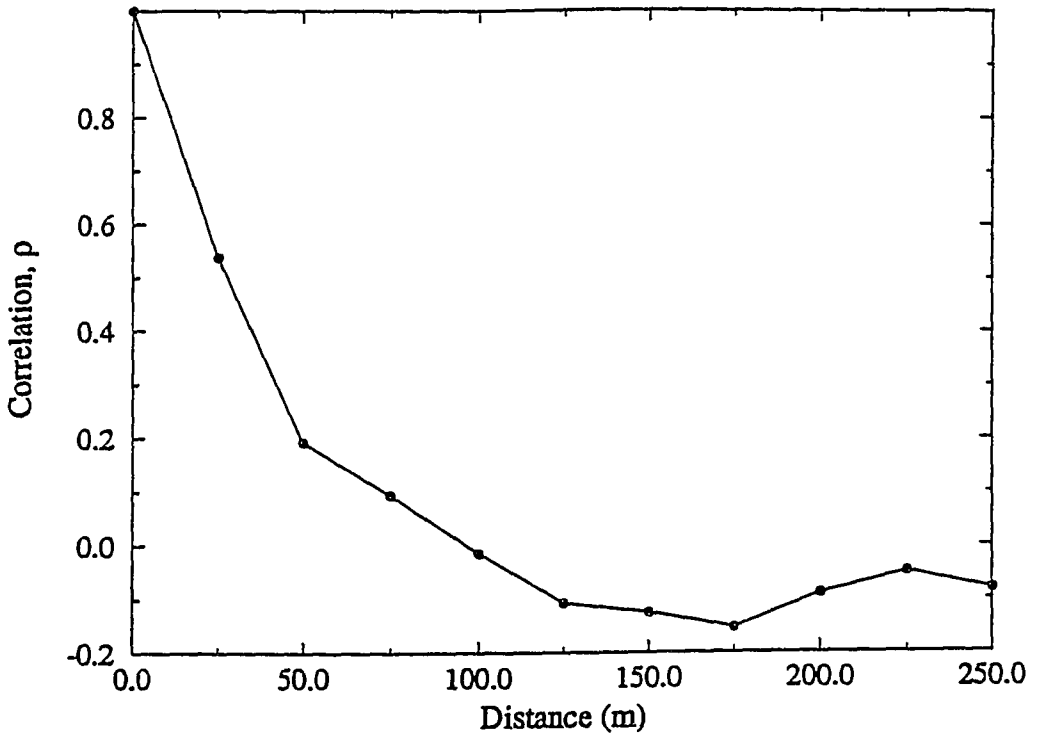

Figure 4.32: Correlation structure of the concentration field (single covariance structure) in the z direction at time, $t = 20$ years

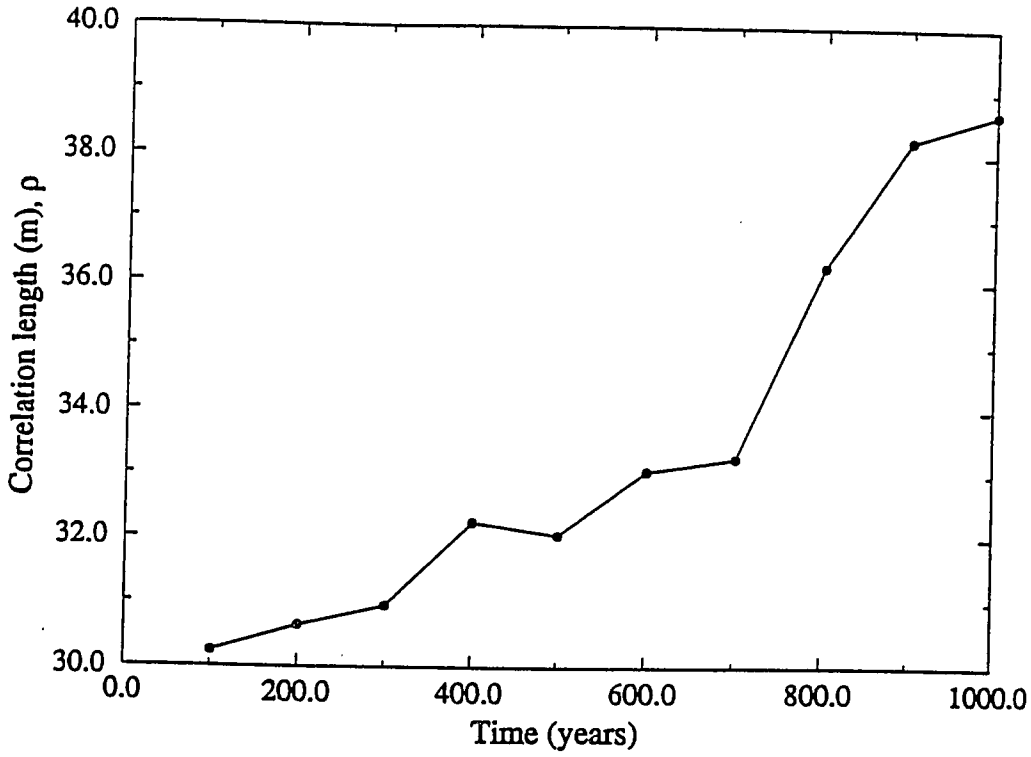

Figure 4.33: Correlation structure of concentration field as a function of time in x direction

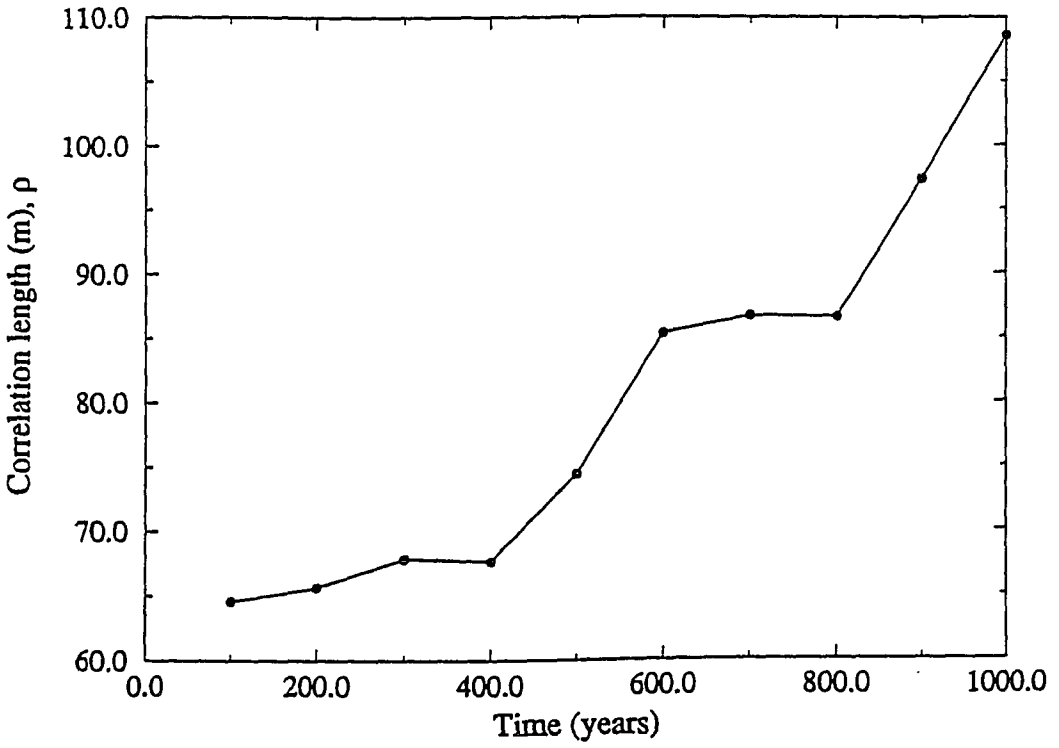

Figure 4.34: Correlation structure of concentration field as a function of time in y direction

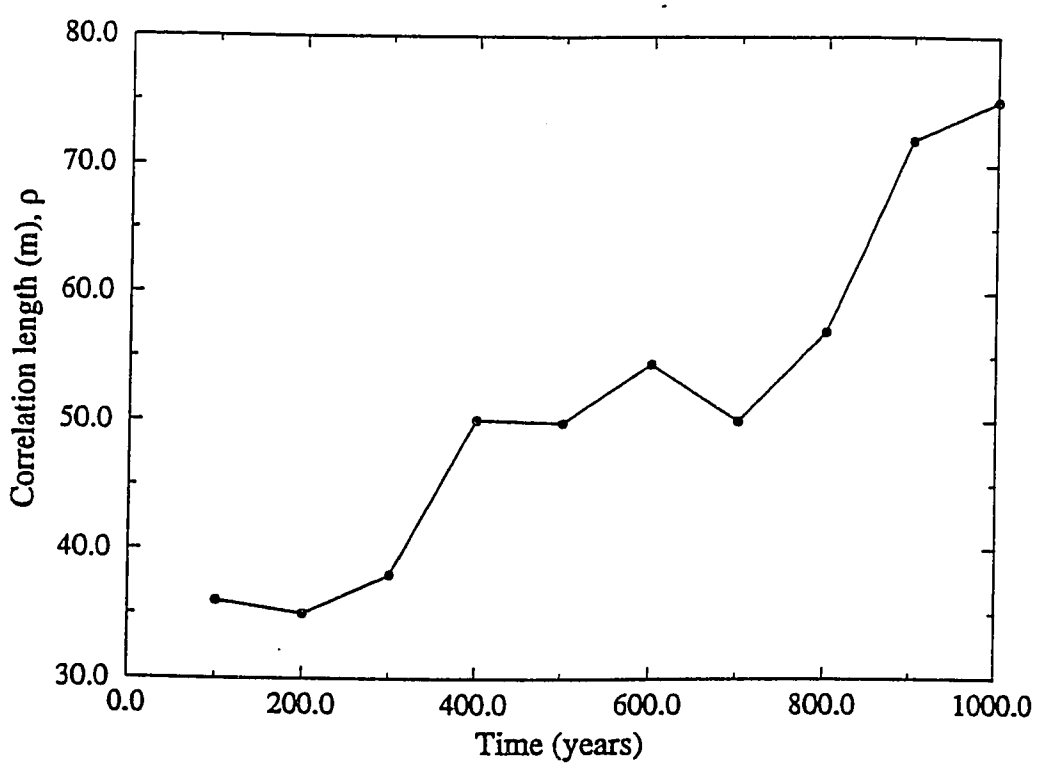

Figure 4.35: Correlation structure of concentration field as a function of time in z direction

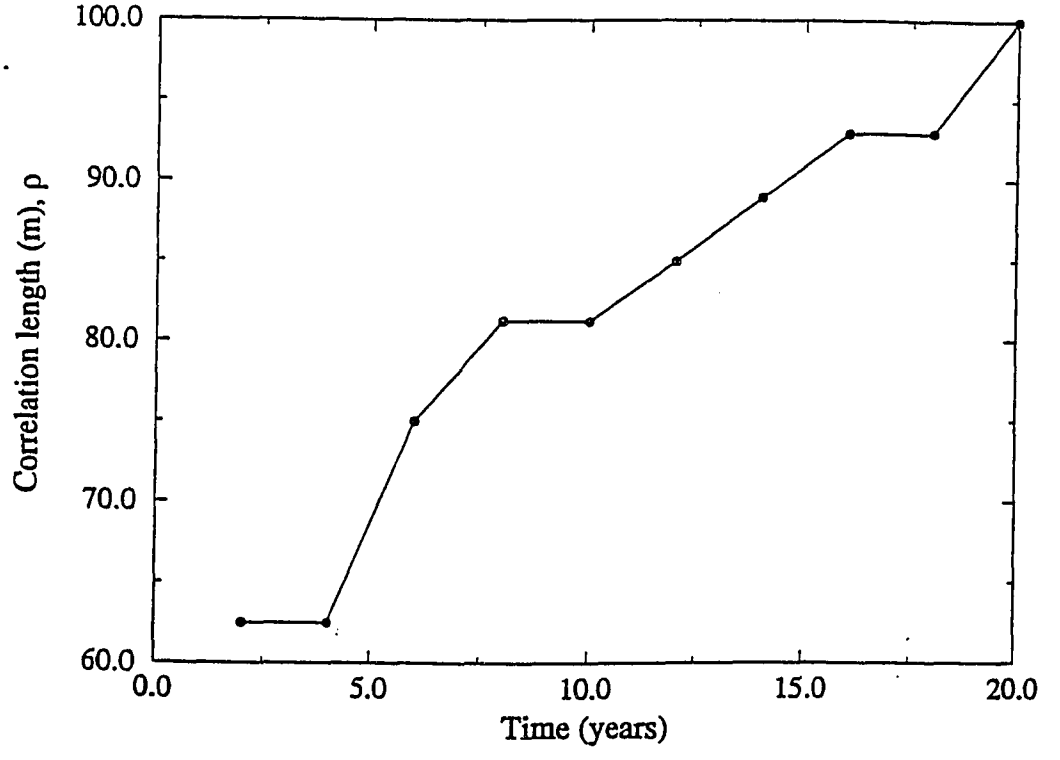

Figure 4.36: Correlation structure of concentration field (single covariance structure) as a function of time in x direction

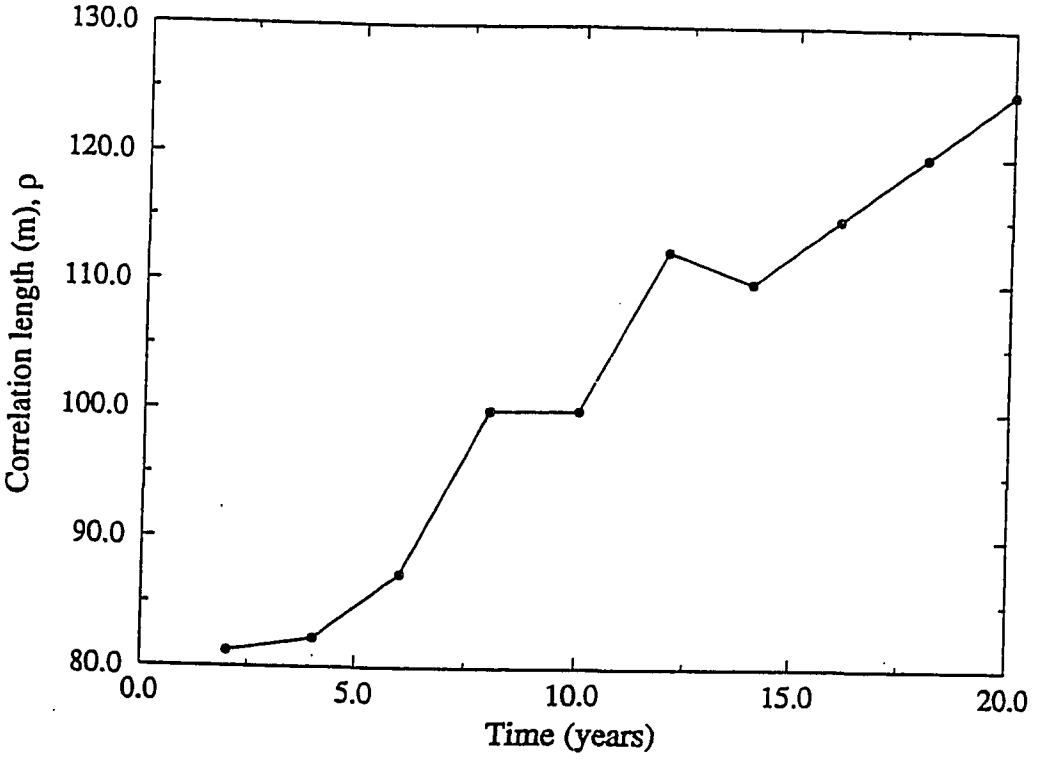

Figure 4.37: Correlation structure of concentration field (single covariance structure) as a function of time in y direction

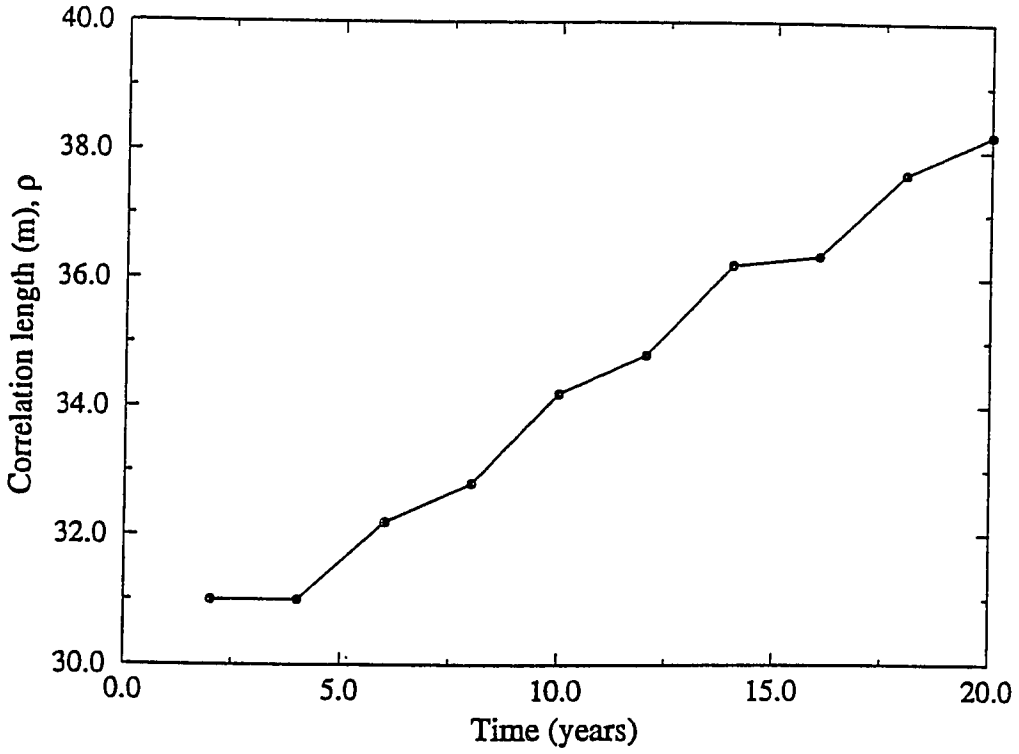

Figure 4.38: Correlation structure of concentration field (single covariance structure) as a function of time in z direction

Chapter 5

CONCLUSIONS

A methodology to incorporate both soft and hard information was developed in order to decrease the uncertainity in the description of the subsurface heterogeneity. The hydraulic conductivity is described as a bimodal distribution with different integral scales, in order to examine the effect of preferential flowpaths on the migration of the contaminant plume. Breakthrough curves were obtained for both the unimodal and bimodal distributions to compare the effect of preferential flow paths on the mean arrival times. Correlation structures of the concentration field was obtained to examine the evolution of the plume in space and time.

Several three-dimensional realizations of the distribution of densely-welded and non-welded tuffs in the volcanic section below a portion of Yucca Flat were generated to demonstrate the SIS methodology. Resistivity was used as the hydrogeologic attribute to indicate the presence of welded tuff verses nonwelded tuff. Welded tuff may act as groundwater flow paths within the volcanic section at Yucca Flat. The simulations demonstrate that resistivity log data works well as an indicator of densely-welded tuffs. The simulated welded

tuffs reproduce the stratigraphic relationships of the welded tuff and vitric tuff aquifers as represented by hydrogeologic cross sections, while incorporating the heterogeneity and anisotropicity that would be expected from these units in a subsurface setting.

The indicator maps generated using the SIS technique was used along with the hydraulic conductivity information available to generate the hydraulic conductivity field conditioned to both the hard and soft information and with different correlation lengths for the welded and non-welded tuff units.

The Particle Tracking Random Walk Method (PTRW) was used to simulate the transport of tritium through a steady state saturated hydrologic system. The concentration plume displayed the effect of preferential flow paths by separating into small blocks and travelling with different velocities. The breakthrough curves also displayed a large tail, suggesting the arrival of few particles at very early time, and then the remaining particles take longer time to cross the breakthrough plane. These simulations very clearly displayed the effect of different geologic materials with different spatial continuity on the contaminant migration. The concentration field from a unimodal distribution of hydraulic conductivity displayed an entirely different result, especially the travel times were much higher in the latter case. This may be due to overestimating of hydraulic conductivity values, when two different materials are present with huge difference in their expected value of hydraulic conductivity.

The concentration fields were dtrended in order to comply with the assumption of stationarity. But still the correlation structures displayed a trend or non-stationarity. Also the concentrations in the transverse directions displayed higher spatial continuity than the longitudinal direction, indicating more spreading in the transverse directions. The

correlation lengths were obtained as a function of time in order to study the evolution of the plume. In all the three directions, the plume seemed to increase the spatial continuity with time.

The final hydraulic conductivity produced using the resistivity values and the hard hydraulic conductivity values reproduced the stratigraphic relationships of the welded tuff and vitric tuff aquifers as represented by hydrogeologic cross sections, while incorporating the heterogeneity and anisotropicity that would be expected from these units in a subsurface setting. They also showed the presence of welded tuff units in the upper boundary, which may act as flow conduits for contaminant migration.

Finally, the hydraulic conductivity field produced based on both soft and hard information, seems to reproduce the stratigraphic relationships of the different materials present and the bimodal distribution has a dramatic effect on the contaminant migration.

Bibliography

[1] Alabert, F.G., Stochastic imaging of spatial distributions using hard and soft information, M.S. Thesis, Appl. Earth Sci. Dept., Stanford University, 184 pp, 1987.

[2] Andricevic, R., and E. Foufoula-Georgiou, Modeling kinetic non-equilibrium using the first two moments of the residence time distribution, Stoch. Hydrol. and Hydraulics, 5, 155-171, 1991.

[3] Bear, J., Dynamics of Fluids in Porous Media, Elsevier, New York, 1972.

[4] Chavent, G., and J.E. Roberts, A unified physical presentation of mixed, mixed-hybrid finite elements and standard finite difference approximations for the determination of velocities in waterflow problems, Adv. Water Resources, 14(6), 329-348, 1992.

[5] Dagan, G., Statistical theory of groundwater flow and transport - Pore to laboratory, laboratory to formation, and formation to regional scale, Water Resour Res., 22(9), 120S-135S, 1986.

[6] Dagan, G., Flow and Transport in Porous Formations, Springer-Verlag, New York, 1989.

[7] Delhomme, J.P., Spatial variability and uncertainity in groundwater flow parameters, A geostatistical approach, Water Resour. Res., 15(2), 269-280, 1979.

[8] Deutsh, C.V. and A.G. Journel, GSLIB: Geostatistical Software Library and User's Guide, Oxford Univ. Press, 340 pp, 1992.

[9] Drellack, S.L., and P.H. Thompson, Selected stratigraphic data for drill holes in LANL use areas of Yucca Flat, NTS, Fenix & Scisson of Nevada Geologic Report, DOE/NV/10322-39, 189pp, 1990.

[10] Gelhar, L.W., Stochastic subsurface hydrology from theory to applications, Water Resour. Res., 22(9) 1355-1455, 1986.

[11] Gomez-Hernandez, J.J., and R.M. Srivastava, ISIM3D: An ANSI-C three dimensional multiple indicator conditional simulation program, Comp & Geo S., 16(4), 395-440, 1990.

[12] Journel, A.G., Fundamentals of geostatistics in five lessons. Short course in Geology, Vol. 8, American Geophysical Union, 40 pp, 1989.

[13] Journel, A.G., and F.G. Alabert, Non-gaussian data expansion in the Earth Sciences, Terra Nova, 1(2), 123-134, 1989.

[14] Morrison, D.T., R. Andricevic, Heterogeneity in Hydraulic Conductivity: Its Impat Upon Solute Transport and Correlation Structures, University of Minnesota, St. Anthony Falls Hydraulic Laboratory, Project Report No. 314, 90pp, 1991.

[15] Morrison, D.T., R. Andricevic and C.M. Wasikowski, Numerical simulation of Two-Dimensional Conservative Solute Transport, International Video Journal of Engineering Research, 2, 73-83, 1992.

[16] Tompson, A.F.B., and R. Abadou and L.W. Gelhar, Applications and Use of Three-Dimensional Turning Bands Random Field Generator, Single Realization Problems, Ralph M. Parsons Laboratory for Water Resources and Hydrodynamics, Massachusetts Institute of Technology, Technical Report Number 313, 1987.

[17] Tompson, A.F.B., and L.W. Gelhar, Numerical Simulation of Solute Transport in Three-Dimensional, Randomly Heterogeneous Porous Media, Water Resour. Res., 26(10), 2541-2562, 1990.

[18] Winograd, I.J., and W. Thordarson, Hydrogeologic and hydrochemical framework, south-central Great Basin, Nevada-California, with special reference to the Nevada Test Site, Professional paper 712-C, U.S. Geol. Survery, 126 pp, 1975.

[19] U.S. Department of Energy, Nevada Operations Office, Office of External Affairs. Annound United States Nuclear Test, July 1945 Through December 1990. Washington, D.C.: U.S. Department of Energy, 1991.

[20] Keys, W.S., 1990. Borehole Geophysics Applied to Groundwater Investigations. TWRI-2-E2, U.S. Geol. Survey, 150 pp.

[21] Drellack, S.L. Jr., 1994. An Introduction to NTS Geology and Geophysical Log Characteristics. Raytheon Services, Nevada, 68 pp.

[22] Blankennagel, R.K. and J.E. Weir Jr. 1973. Geohydrology of the Eastern Part of Pahute Mesa, Nevada Test Site, Nye County, Nevada. U.S. Geological Survey Professional Paper 712-B, 35 pp.

[23] Switzer, P., 1977. Estimation of Spatial Distributions from Point Sources with Application to Air Pollution measurements: Bull. Int. Statist. Inst., v.47, p.123-137.

[24] Journel and Huijbregts, 1978. Mining Geostatistics, Academic Press, London, 600 pp.

[25] Journel, A.G., 1983. Non-parametric Estimation of Spatial Distributions: Math. Geol., v. 15, pp. 445-468.

[26] Freeze, R.A., 1975. A stochastic-conceptual analysis of one-dimensional groundwater flow in nonuniform homogeneous media, Water Resources Research, Vol. 11, pp. 725-741.

[27] Hoeksema, R.J. and P.K. Kitanidis, 1985. Analysis of the spatial structure of properties of selected aquifers, Water Resources Research, Vol. 21, pp. 563-572.

[28] Sudicky, E.A., 1986. A natural gradient experiment on solute transport in a sand aquifer: Spatial variability of hydraulic conductivity and its role in the dispersion process, Water Resources Research, Vol. 22, pp. 2069-2082.

[29] Mose, R. and P. Siegel, and P. Ackerer., 1994. Application of the mixed hybrid finite element approximation in a groundwater flow model: Luxury or necessity ?, Vol. 30, No. 11, pp. 3001-3012.

[30] Huyakorn, P.S. and G.F. Pinder, 1983. Computational Methods in Subsurface Flow. Academic Press, San Diego.

[31] Kinzelbach, W., 1988. The random walk method in pollutant transport simulations, Groundwater Flow and Quality Modeling. E. Custodio, A. Gurgui, and J.P.L. Ferreira (Eds.). D. Reidel, Hingham, Massachusetts.

[32] Prickett, T.A., T.G. Naymik, and C.G. Lonnquist, 1981. A random walk solute transport model for selected groundwater quality evaluation, Illinois State Water Survey Bulletin 65, Champaign, Illinois.

[33] Ababou, R., L.W. Gelhar, and D. McLaughlin, 1988. Three-dimensional flow in random porous media, Technical Report Number 313, Volumes 1 and 2, R.M. Parson Laboratory, Department of Civil Engineering, M.I.T., Cambridge, Massachusetts.

[34] Singh, A. and A.K. Singh, 1994. Trend Removal in Spatially Correlated Data Sets, Math Geology.

[35] Istok, J.D., C.A. Rautman, L.E. Flint and A.L. Flint, 1994. Spatial variability in hydrologic properties of a volcanic tuff. Groundwater, 32(5), 751-760.

[36] Rubin, Y., Mavko, G., and Harris, J., 1992, Mapping permeability in heterogeneous aquifers using hydrologic and seismic data, Water Resources Research, 28(7), 1809-1816.

[37] Copty, N., Y.Rubin, and G. Mavko, 1993, Geophysical hydrological identification of field permeabilities through Bayseain updating, Water Resources Research 29(8), 2813-2825.

[38] Philips, F.M., and Wilson, J.L., 1989, An approach to estimating hydraulic conductivity spatial correlation scales using geological characteristics, Water Resources Research, 25(1), 141-143.

[39] Rubin, Y., and Journel, A.G., 1991, Simulation of Non-Gaussian Space Random Functions for Modeling Transport in Groundwater, Water Resources Research, 27(1), 1711-1721.

[40] Branna, J.R. and Haselow, J.S., 1993, Compound random field models of multiple scale hydraulic conductivity, Water Resources Research, 29(2), 365-372.

[41] Ritzi, R.W., D.F. Jayne, A.J. Zahradnik, Jr., A.A. Field, and G.E. Fogg, 1994, Geostatistical modeling of heterogeneity in glaciofluvial, buried-valley aquifers, Groun Water, 32(4), 666-674.

[42] Wingle, W.L., E.P. Poeter, and S.A. McKenna, 1994, UNCERT User's Guide, Draft, developed for U.S. Bureau of Reclamation, Colorado School of Mines, Golden, CO.